NICST Internal Memo

Date: October 25, 2010
From: Jeff McIntire and Tom Schwarting
To: Bruce Guenther, Jim Butler, and Jack Xiong
Subject: Updated Analysis of VIIRS F1 RSR

References:

[1] NICST_MEMO_10_002, 'Analysis of VIIRS F1 Relative Spectral Response for the LWIR FPA,' J. McIntire, T. Schwarting, N. Che, and C. Pan, February 22, 2010.
[2] NICST_MEMO_10_007, 'Analysis of VIIRS F1 Relative Spectral Response for the SMWIR FPA,' J. McIntire, T. Schwarting, N. Che, C. Pan, and A. Wu, April 14, 2010.
[3] NICST_MEMO_10_017, 'Updated Analysis of VIIRS VisNIR Relative Spectral Response,' T. Schwarting, J. McIntire, and C. Pan, June 21, 2010.
[4] 'Sensor Performance Verification Plan,' PVP154640-101.
[5] 'Performance Specification Sensor Specification,' ps154640-101c.

1. Introduction

During the fall of 2010, the government team RSR splinter group (composed of members from the University of Wisconsin, NICST, Aerospace Corp, and MIT Lincoln Labs) converged and updated their analysis to produce the "Government Best RSR" for VIIRS F1 sensor. The government team's efforts were directed solely on the RSR measured during instrument level, Thermal Vacuum testing in the summer of 2009; RSR derived from the spacecraft level testing with the Traveling SIRCUS will not be discussed in this work.

The "Government Best RSR" is equivalent to NICST version 3 RSR. The processing and analysis that was performed to produce the version 2 RSR was detailed in [1-3]. This memo will detail the improvements undertaken by the government team both in terms of processing and results.

2. Analysis

2.1 Improved SNR filtering

The major improvement in the RSR processing included in this memo is the update to the SNR filtering. SNR filtering was used in [1,2] to ensure that the Relative Spectral Output (RSO) of the SpMA was not scaling features which were essentially noise. The filtering was originally set such that any point with a SNR greater than 3 was scaled by the RSO. Note that this filtering was only applied to the RSR in the cold focal planes. However, it was clear some real features were below this threshold. Because of the detector to detector variation, it was difficult to set a single filter threshold per band. As a result, the band averaged SNR was introduced.

The band averaged SNR was used as an improved method of discriminating which points were real features of the RSR and which were noise. It was noticed that the noise features tend to fluctuate around zero as a function of detector whereas real features were generally biased on average to a positive value. In consequence, by averaging the SNR over detectors, the noise features are driven lower, while the real features tend to be more stable. As a result, it becomes much easier to set thresholds to differentiate between noise and real RSR features.

The band averaged SNR is determined as follows: the standard deviation of all samples in each scan is determined (using a three sigma rejection for all bands except I1 and I2, which use a six sigma rejection); then the average standard deviation is calculated for both shutter open and shutter closed scans; next, the noise is determined as the root sum square of the shutter open and closed averages; the SNR is the dn divided by the noise and the band averaged SNR is the SNR averaged over all detectors in a given band. Note that the band averaged SNR is used solely as a tool for discriminating real RSR features from noise.

Table 1 gives the band averaged SNR filter thresholds used in this work for all bands. Note that SNR filter thresholds are now used for the VisNIR bands (none were used in version 2). Figure 1 displays the version 2 and 3 RSR for band I1, detector 16 (black and red curves, respectively). The differences in RSR below 420 nm and about 700 nm are due to noise features no longer being scaled. There is also some difference near the IB region; this is the result of a error in the VisNIR stitching algorithm which will discussed in a later section (2.3). The band averaged SNR for I1 is plotted in Figure 2 (note the dashed red line indicating the SNR filter threshold).

Figures 3 – 44 show the RSR (detector 9 for M bands and detector 16 for I bands) and the band averaged SNR for each band in the same manner as Figures 1 and 2 for band I1. For the cold focal plane RSR, a dashed blue line indicating the previous SNR filter threshold of 3 is also included. Note that for the VisNIR bands, the differences between versions 2 and 3 are largely confined to the noise floor (typically below 400 nm and above 1000 nm). However, in the case of the cold focal planes, some features that were not scaled by the RSO in version 2 are in version 3. For I3 (Figures 5 and 6), the features in the 1700 to 2300 nm region were affected. In M8 (Figures 25 and 26), wavelengths from 2000 to 2600 nm as well as from 3500 to 4000 nm are now scaled by the RSO. Similar results were seen in bands M9, M10, and M11 (Figures 27-32). It has been suggested that the features in some of the SWIR bands between 3500 and 4500 nm may be the possible result of higher order diffraction in the double monochromator (and subsequently being transmitted though the order filters). If this is the case, these features would not be part of the true RSR; this possibility is still under investigation.

In the thermal bands, most of the changes occur near the IB regions below the 10^{-3} response level. The updated SNR filtering now ensures that this data is scaled by the RSO. In addition, there are significant OOB leaks in the 8 – 9 µm region in M15, M16A, and M16B. Only portions of these features were scaled in the version 2 RSR. In the version 3 RSR, the RSO scaling is now applied more completely. However, the RSO tends to scale these points lower; the result is that the IOOB will decrease (as will be seen in section 2.4).

2.2 Atmospheric Effects

Two bands require some consideration of atmospheric effects impacting the RSR data. The first is M9; the atmospheric correction for water vapor effects was implemented by Chris Moeller of the University of Wisconsin. This correction was applied only to the IB measurements (as seen in Figure 45 for detector 9). In addition, because the water vapor effect is temporally dependent, it is difficult to accurately measure the ND filter transmission. This caused a jagged response curve in version 2 RSR as in Figure 46 (black line) at 1355 and 1395 nm, where the stitching of FP-15 to FP-16 occurred. As a result, the stitching in version 3 RSR for this band was conducted below the SNR of 3 point used previously [2]. The version 2 stitching points were 1357 and 1395 nm while the version 3 stitching points were 1350 and 1397 nm. As seen in Figure 46, the version 3 RSR (red curve) removed the jagged features.

The other band where atmospheric effects play a role is M13. In the region of 4200 – 4300 nm, there are some CO_2 absorption features. In Figure 47, the uncorrected version 2 RSR is shown along with atmospheric transmission data. Note that the central spike in the absorption feature corresponds to a decrease in the CO_2 absorption. The transmission data was provided by Chris Moeller of the University of Wisconsin using data taken from a forward model run of the Line-by-Line-Radiative-Transfer-Model. However, these absorption features are at a low response level (between 0.1 and 0.001 % of the peak response). As a result, it is difficult to use an atmospheric model to make a correction (in addition, there was no monitoring of the CO_2 levels in the lab). Instead, a linear fit to the log of the response was performed between the response points at 4177, 4184, 4253, 4260, 4314, and 4321 nm (these points correspond to two points on either edge of the feature and two points in the small sub peak at around 4250 nm). This fit is used to interpolate points across the region of the absorption feature. The resulting version 3 RSR for detector 9 is shown in Figure 48 in the absorption region (along with the version 2 RSR).

2.3 VisNIR Stitching and M12

The error in the algorithm for the VisNIR processing was discovered governing the conditions for stitching FP-15 to FP-16. The result was FP-15 data was being retained in the version 2 RSR much lower than the SNR=3 stitch point. The current results implement the stitching as described in [3]. The updated curves for bands I1, M2, M3, and M7 are shown in Figures 49 – 52. The resulting version 3 curves had no effect on any of the IB metrics (center wavelength, bandwidth, or 1 % response points) and little impact on the integrated metric, as will be seen in section 2.4.

The gain for M12 detector 1 is much lower than for other M12 detectors; as a result, the same radiance will produce a much lower signal. The response for M12 detector 1 was much smaller than other detectors in M12, particularly on the short side of the peak. For version 3, the M12 detector 1 RSR at the points between roughly 3350 and 3450 nm was replaced with the RSR from M12 detector 3. The resulting version 3 RSR is shown in Figure 53.

2.4 Effect on Integrated Metric

The IOOB metric (as defined in [1-3]) was used to estimate the amount of light reaching the detectors due to OOB filter leaks assuming a simulated spectrum comprised of solar illumination diffusely reflected off the Earth and the emission of the Earth. As a check on the overall effect of the changes described above, the IOOB derived from NICST versions 2 and 3 are compared.

Figures 54 – 57 show the IOOB for each band versus detector. The dashed red line indicates the specification for a particular band [4,5]. For the VisNIR, the IOOB showed some variation from versions 2 to 3 due to an error in the IOOB calculation (particularly in M1). The changes in the RSR were largely in the scaling of the noise floor and the RSO scaling is generally not large for the VisNIR, so the effect on the IOOB was small.

The correction for the atmospheric effects in bands M9 and M13 had a large impact on the IOOB. For M9, the IOOB decreased by between 0.1 and 0.3 % primarily due to improvements in the stitching. For M13, the IOOB increased by between 0.4 and 0.5 %; in version 2, the atmospheric feature was retained, which had the effect of underestimating the OOB contribution from the 4200 – 4300 nm region. Note that M13 still meets the specified limit on IOOB (1.3 % [5]). In general, the remaining SMWIR bands show little change between the RSR versions. The differences in where the RSO scaling was applied usually occur at low response levels; as a result, the IOOB was not affected much.

In the LWIR, the IOOB for M15, M16A, and M16B all decreased by about 0.05 %. For these bands, some of the features determined to be real in section 2.1 were scaled downward by the RSO, and as such decreased the total OOB contribution. However, these bands were still non-compliant with the specifications (0.4 % each [5]). In the case of I5, the IOOB for the even detectors increased slightly while the odd detectors were largely unchanged. As stated before [1], the even detectors are largely non-compliant due to an incorrect SpMA setting (the slit width was too narrow during the OOB measurement and as a result, the even detectors did not receive enough signal to drive down the noise). The IOOB for M14 was largely unchanged.

3. Summary

The “Government Best RSR” for VIIRS F1 sensor was developed by the government team (University of Wisconsin, NICST, Aerospace Corp, and MIT LL). This corresponds to NICST version 3 RSR. The following improvements over version 2 [1-3] were implemented:

- Improved application of the SpMA RSO. Band averaged SNR was used to set the SNR filter thresholds for application of the RSO. The band averaged SNR allowed for better discrimination between real RSR features and noise;
- Atmospheric effects were corrected in bands M9 (water vapor) and M13 (CO_2);
- Algorithm errors in the stitching of FP-15 to FP-16 and IOOB calculation were corrected in the VisNIR bands;
- and M12 detector 1 RSR between 3350 and 3450 nm replaced by detector 3 RSR due to low SNR.

The effects of the improvements incorporated in the version 3 RSR on the IOOB are largest for bands M9, M13, M15, M16A, and M16B. For bands M9 and M13, the difference is the result of updated treatment of the atmospheric features. For bands M15, M16A, and M16B, the improved application of the SpMA RSO resulted in a slight decrease in IOOB. Compliance with the specifications is unchanged from [1-3].

Acknowledgement

The sensor test data used in this document was provided by the Raytheon El Segundo testing team. Approaches for data acquisition and data reductions, as well as data extraction tools were also provided by the Raytheon El Segundo team. We would like to thank the Raytheon El Segundo team for their support. The data analysis tools were developed by the NICST team.

Table 1: SNR filter thresholds

Band	SNR Filter Threshold
I1	0.05
I2	0.04
I3	0.05
I4	0.05
I5	0.2
M1	0.02
M2	0.02
M3	0.03
M4	0.04
M5	0.02
M6	0.015
M7	0.022
M8	0.03
M9	0.025
M10	0.04
M11	0.03
M12	0.07
M13	0.03
M14	0.3
M15	0.17
M16A	0.17
M16B	0.15

Figure 1: I1 RSR from NICST versions 2 and 3

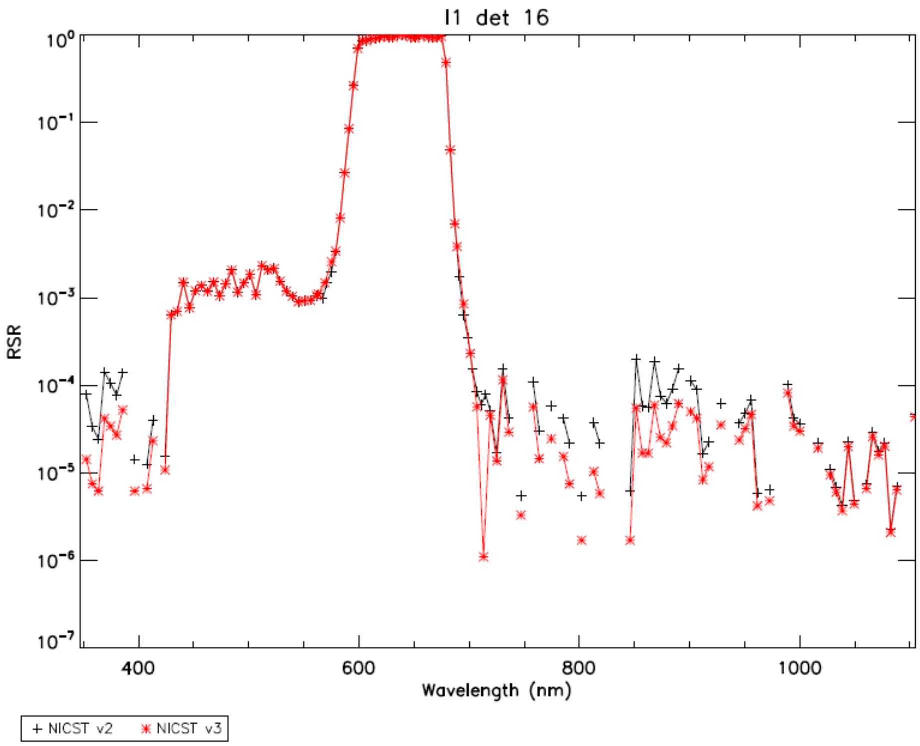

Figure 2: I1 band averaged SNR from NICST version 3

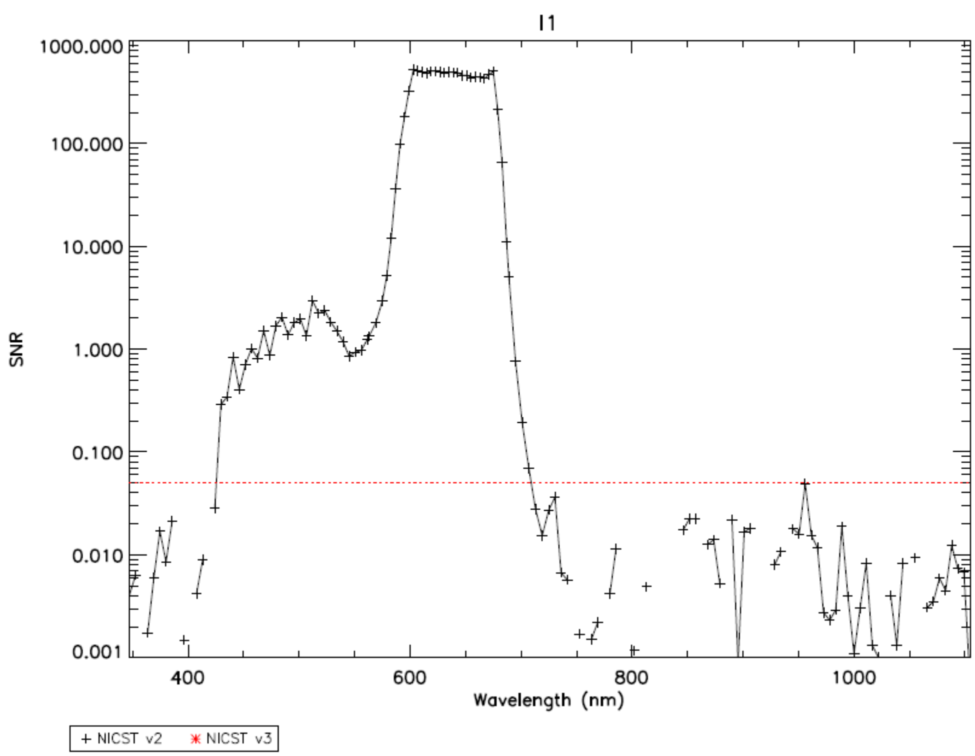

Figure 3: I2 RSR from NICST versions 2 and 3

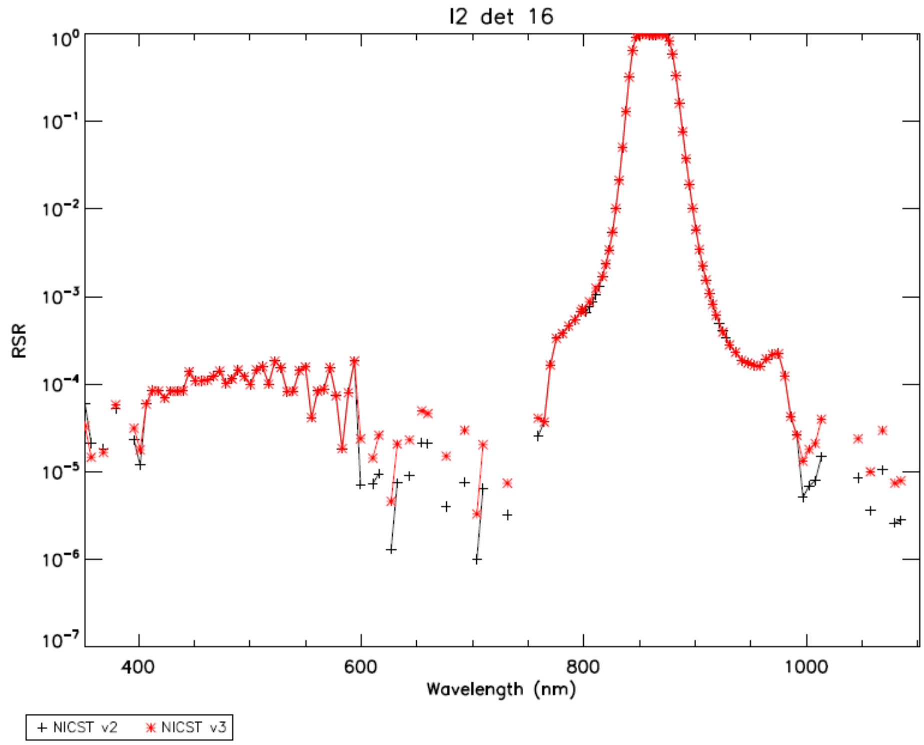

Figure 4: I2 band averaged SNR from NICST version 3

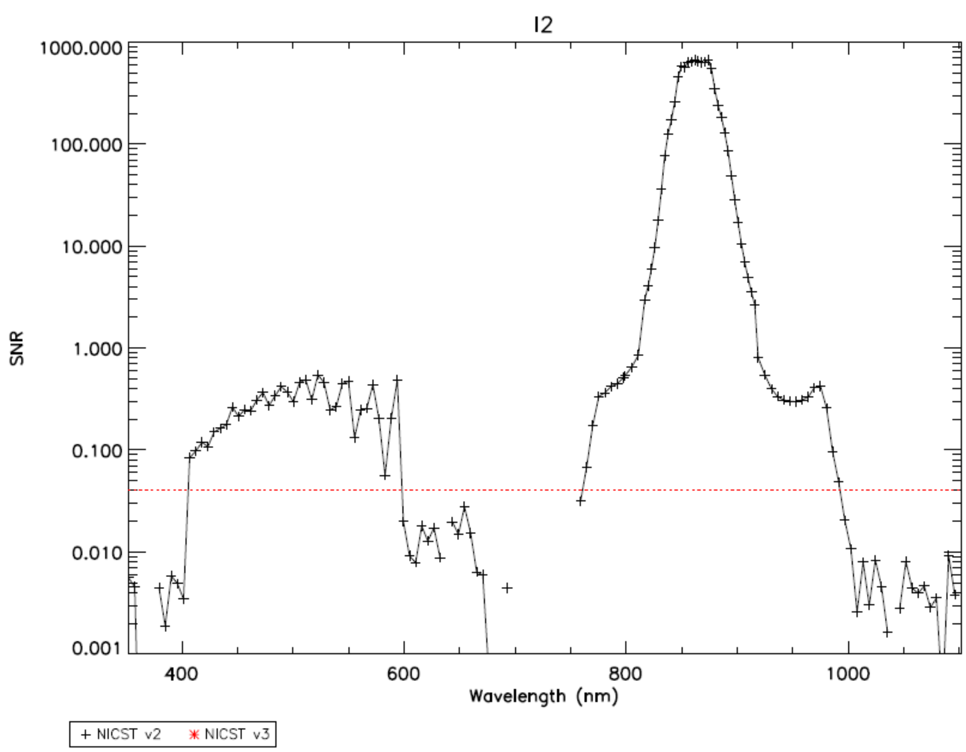

Figure 5: I3 RSR from NICST versions 2 and 3

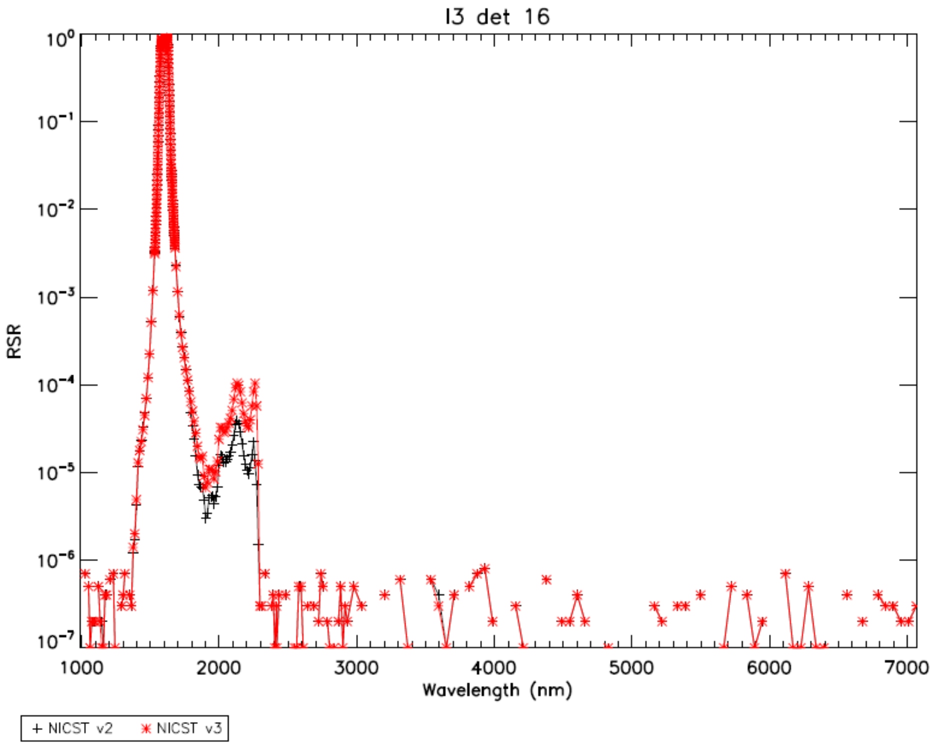

Figure 6: I3 band averaged SNR from NICST version 3

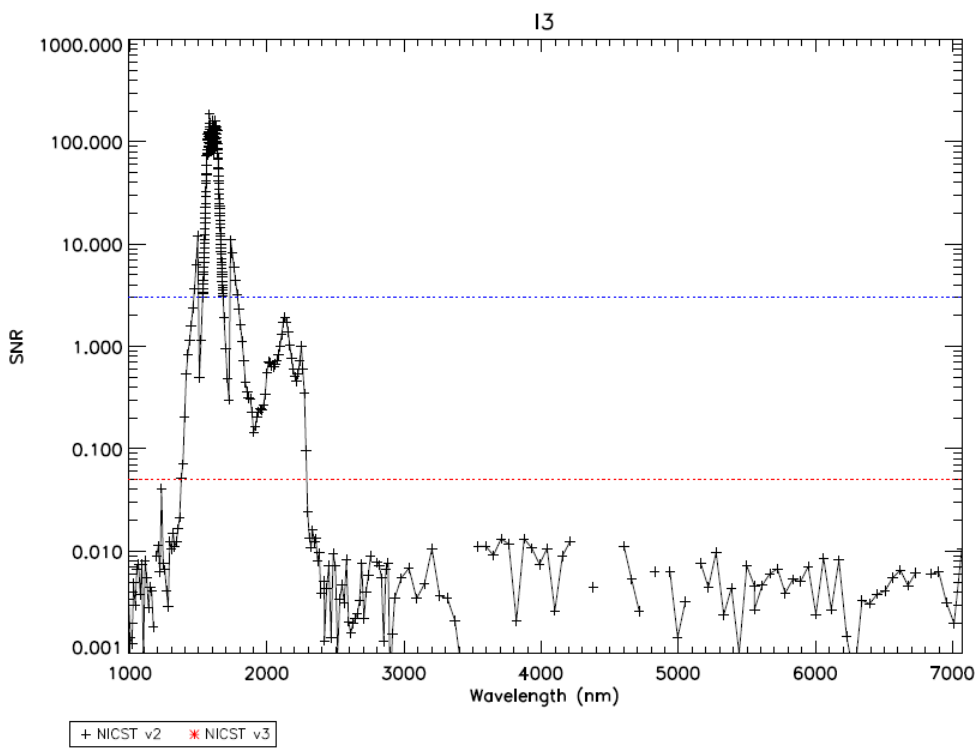

Figure 7: I4 RSR from NICST versions 2 and 3

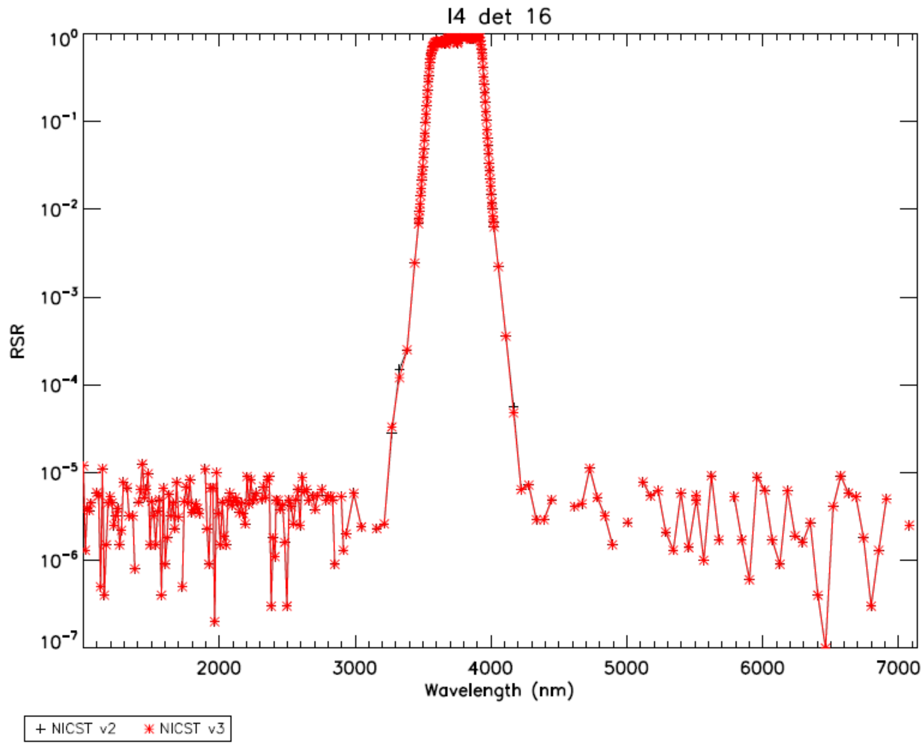

Figure 8: I4 band averaged SNR from NICST version 3

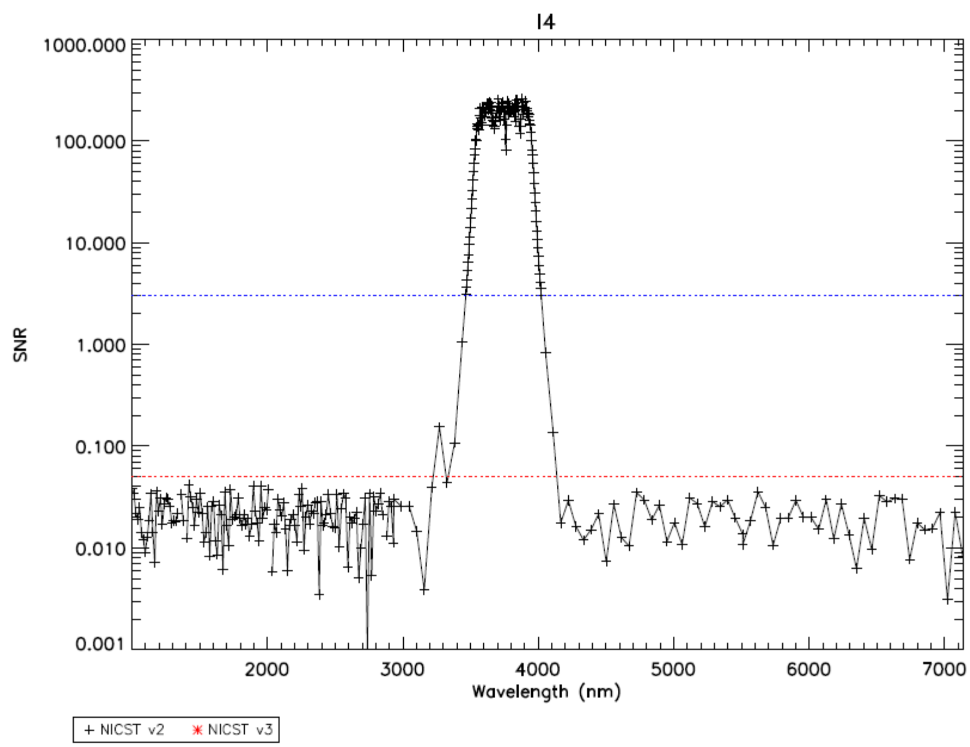

Figure 9: I5 RSR from NICST versions 2 and 3

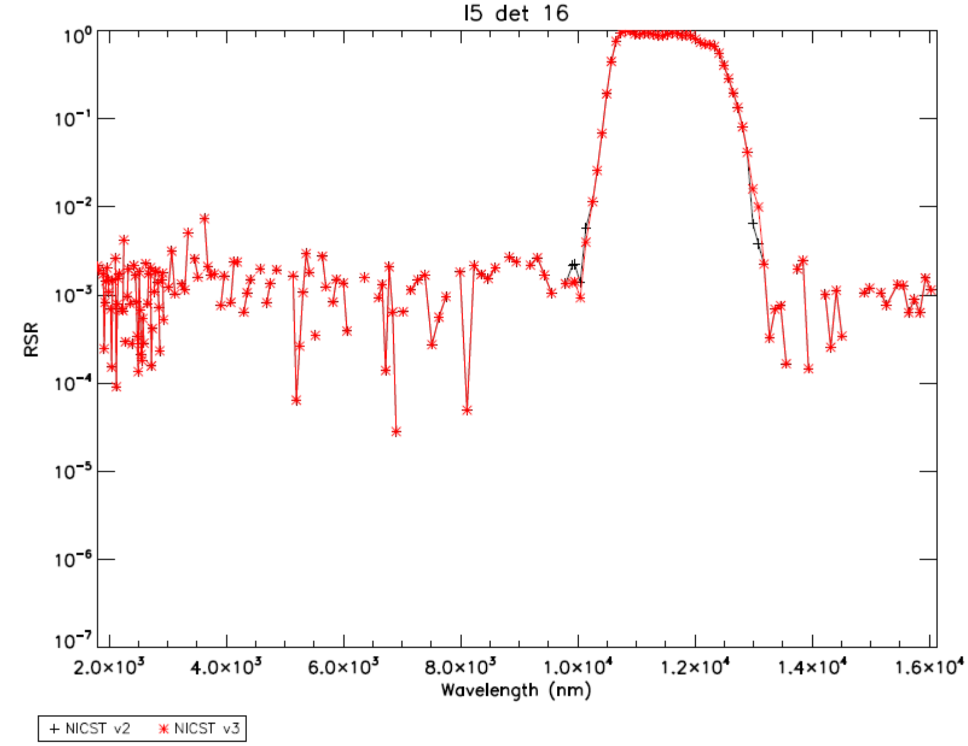

Figure 10: I5 band averaged SNR from NICST version 3

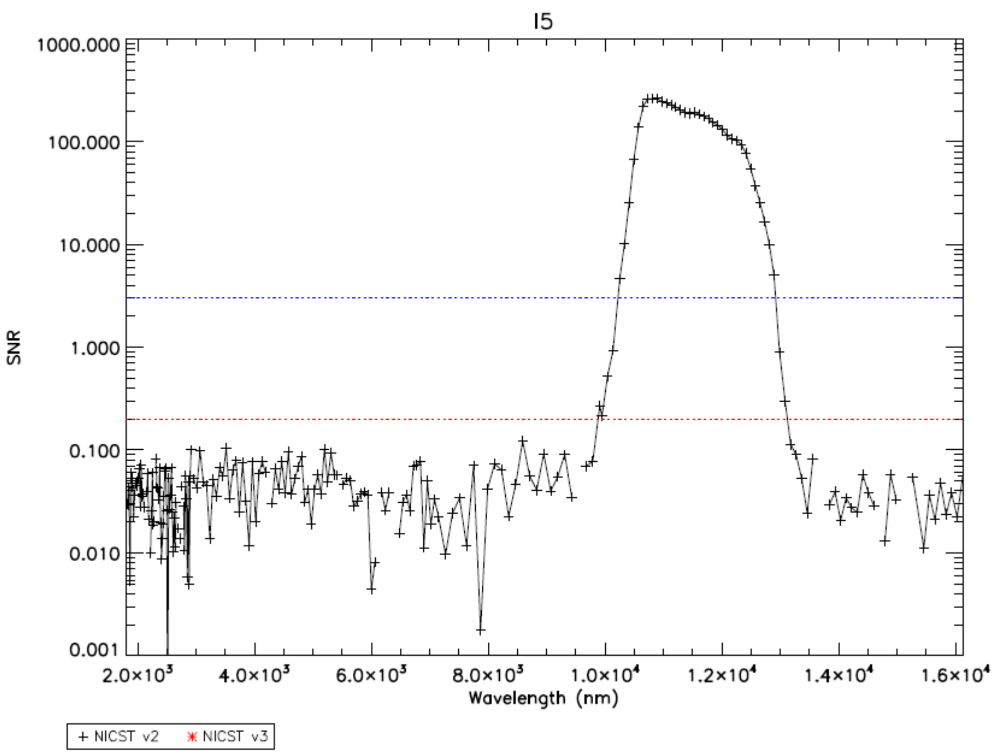

Figure 11: M1 RSR from NICST versions 2 and 3

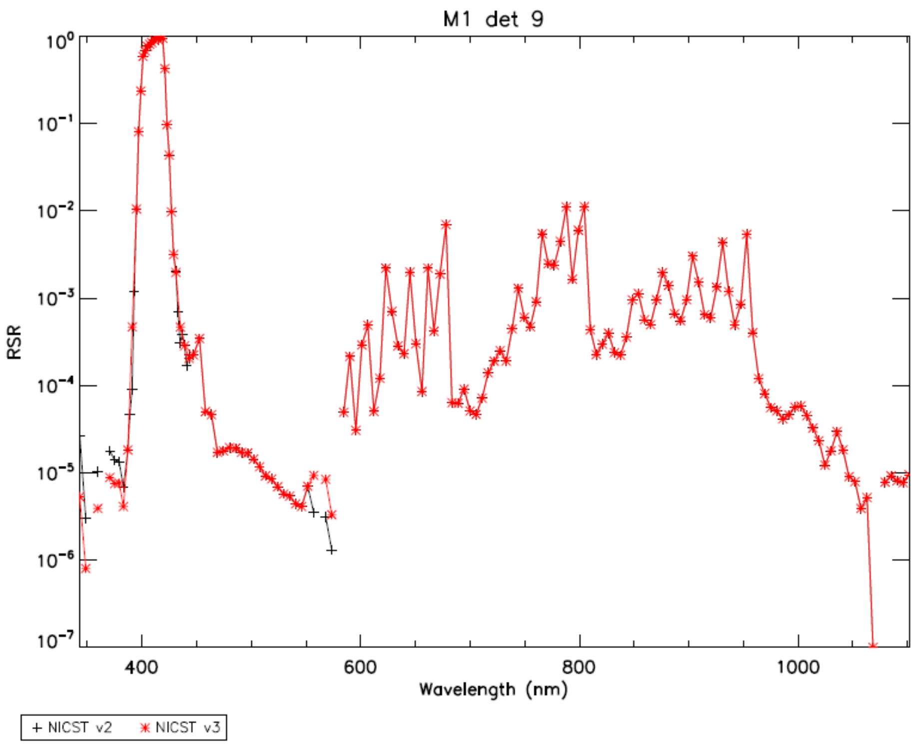

Figure 12: M1 band averaged SNR from NICST version 3

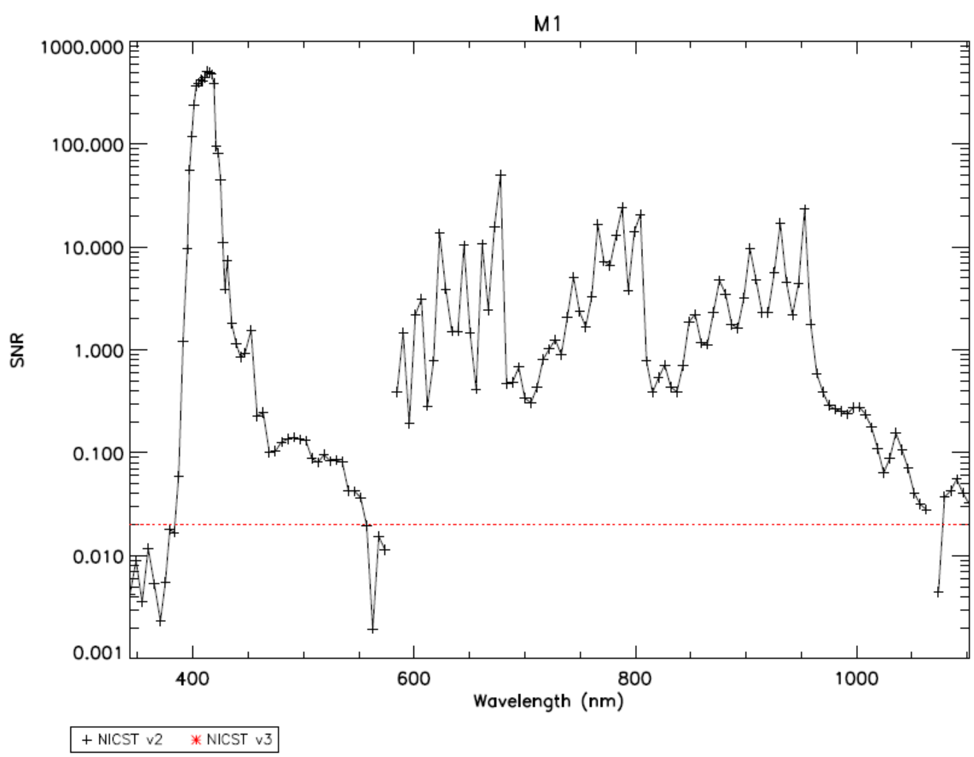

Figure 13: M2 RSR from NICST versions 2 and 3

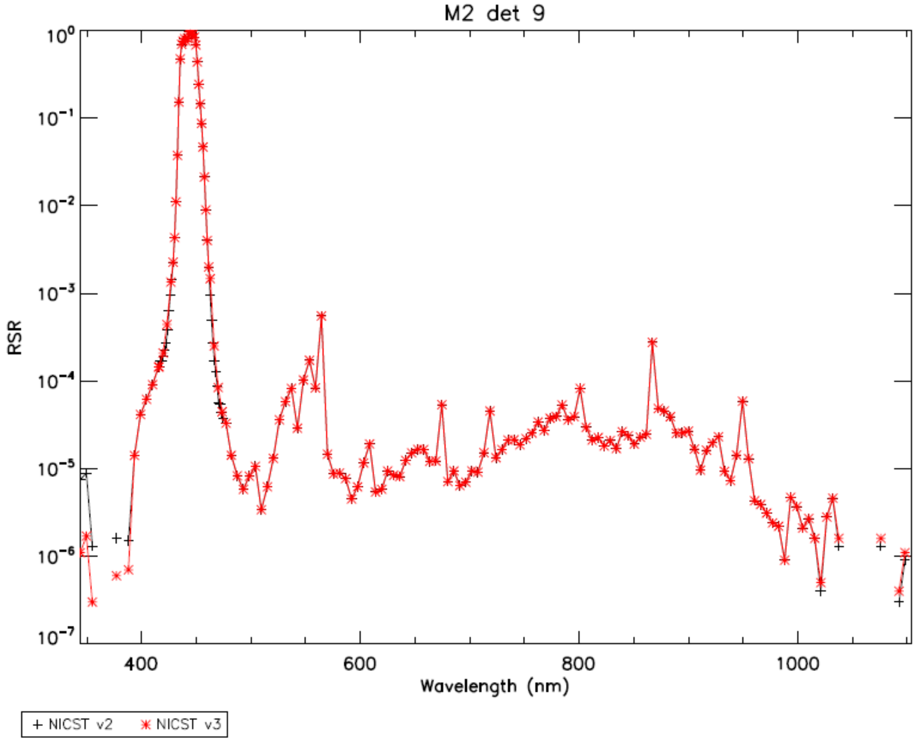

Figure 14: M2 band averaged SNR from NICST version 3

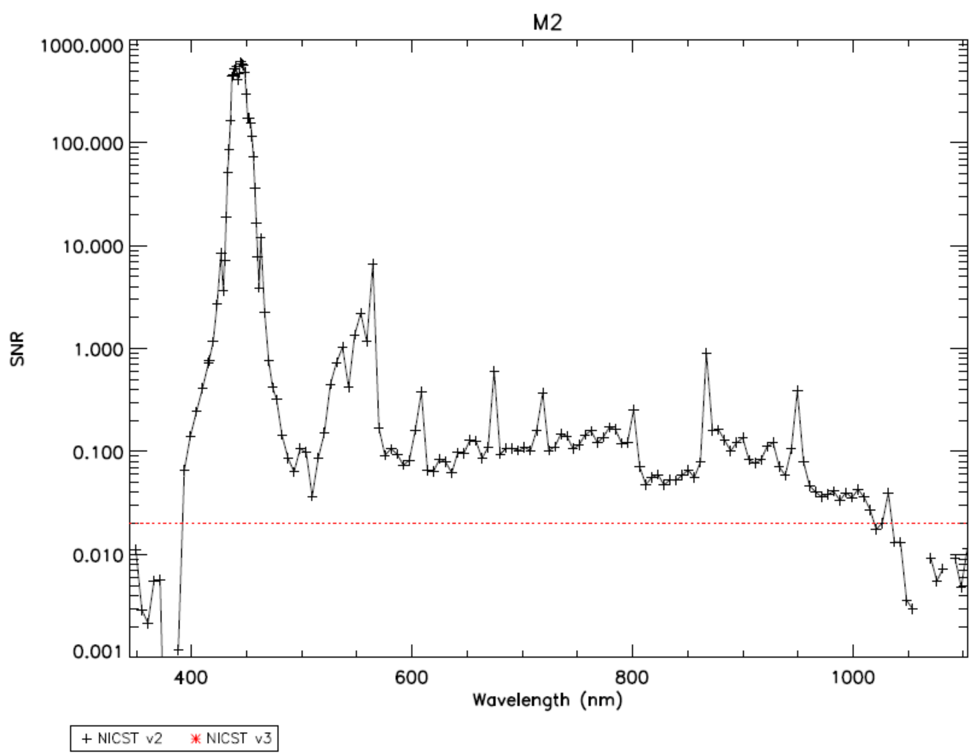

Figure 15: M3 RSR from NICST versions 2 and 3

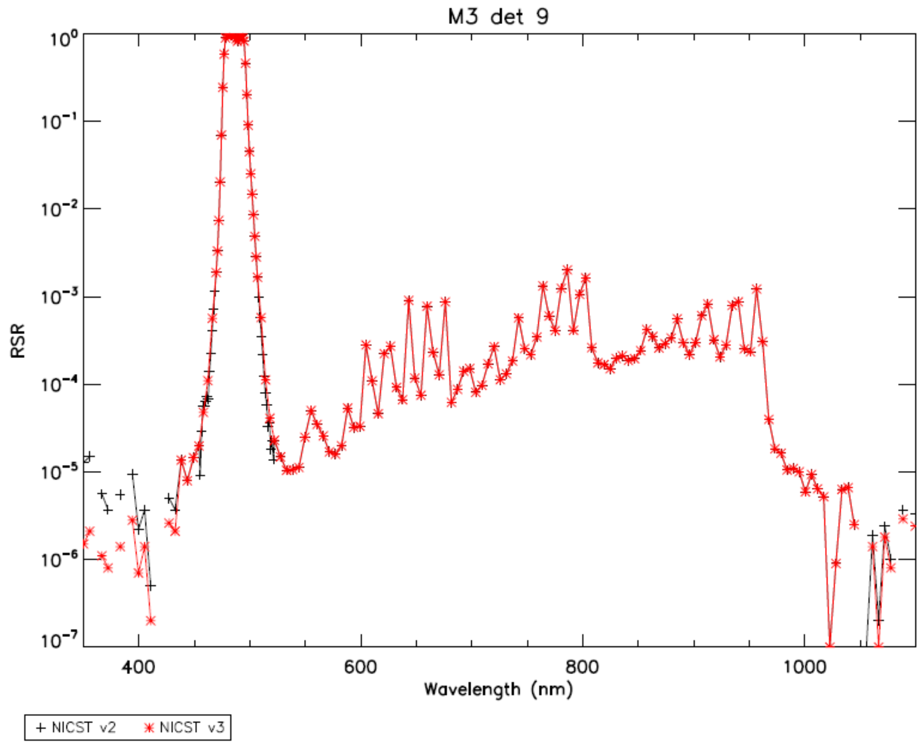

Figure 16: M3 band averaged SNR from NICST version 3

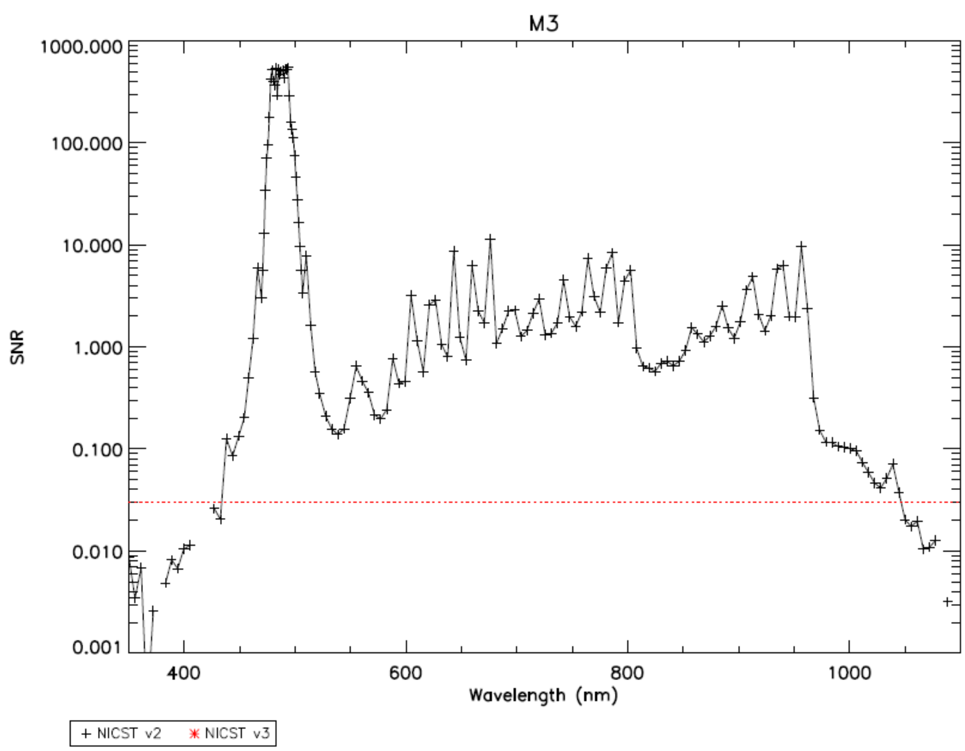

Figure 17: M4 RSR from NICST versions 2 and 3

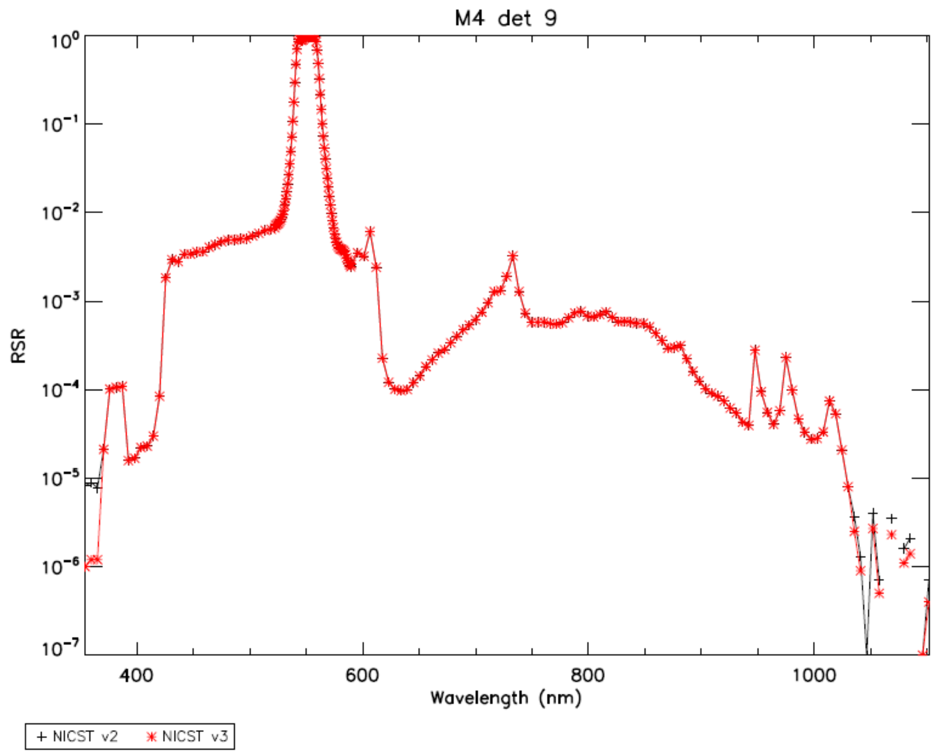

Figure 18: M4 band averaged SNR from NICST version 3

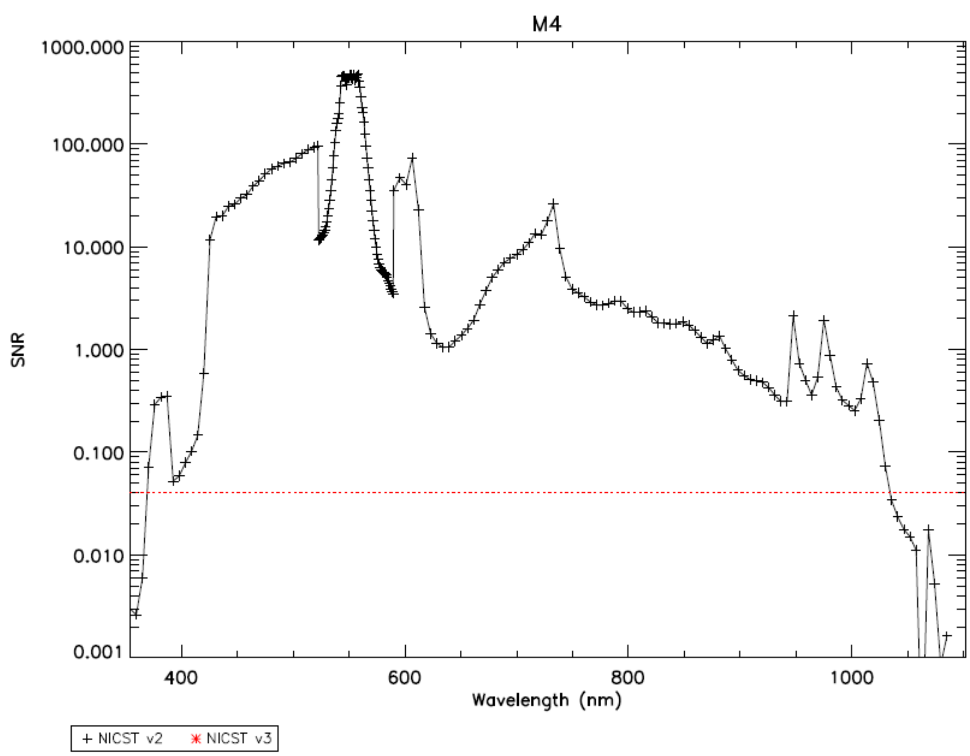

Figure 19: M5 RSR from NICST versions 2 and 3

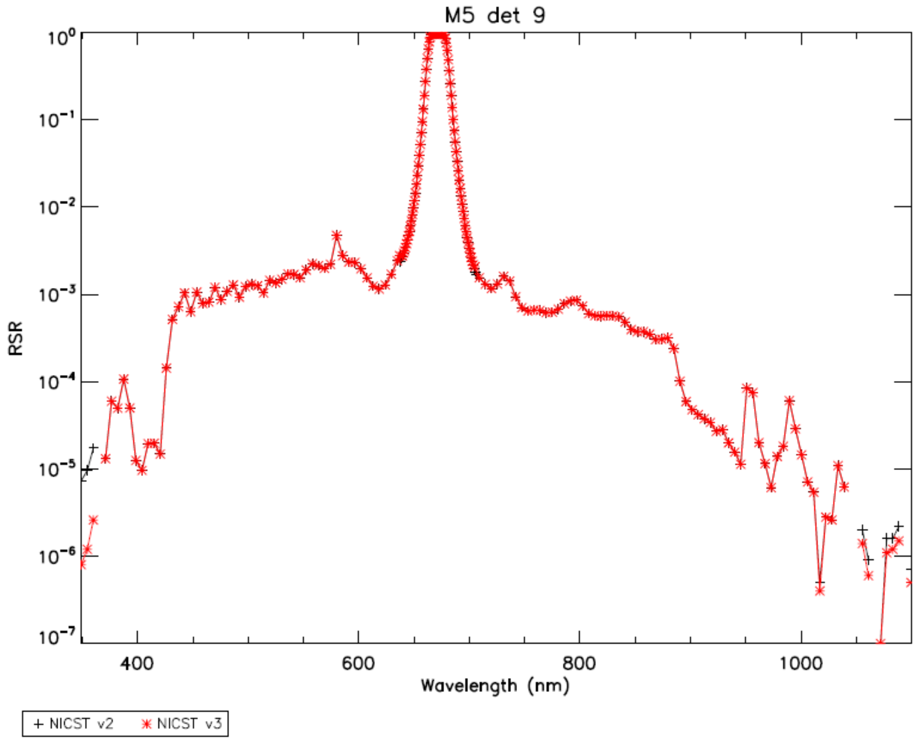

Figure 20: M5 band averaged SNR from NICST version 3

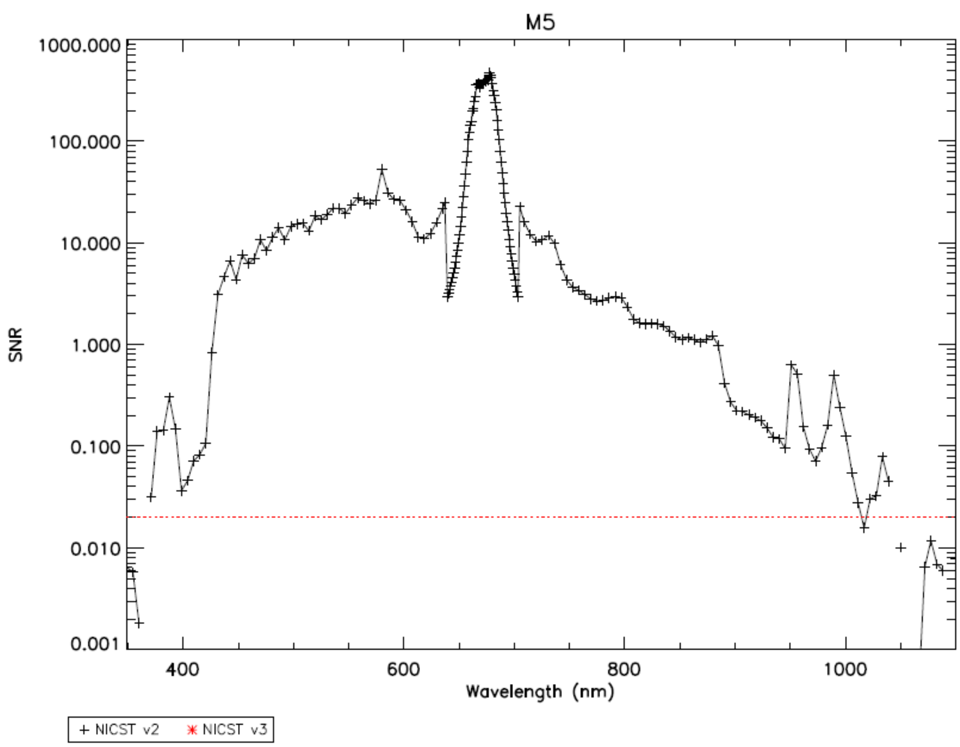

Figure 21: M6 RSR from NICST versions 2 and 3

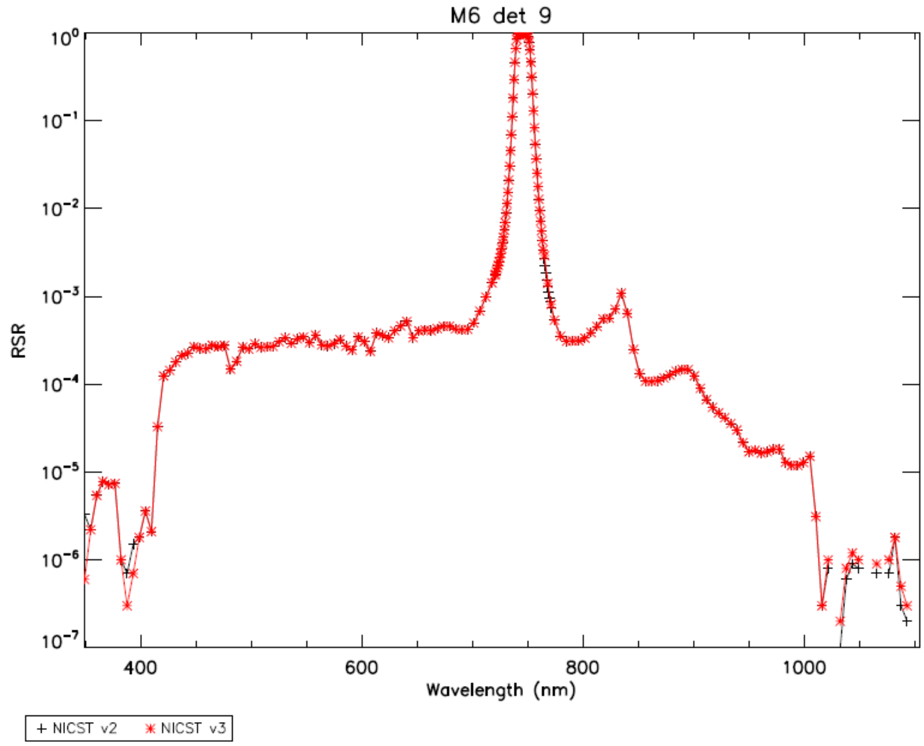

Figure 22: M6 band averaged SNR from NICST version 3

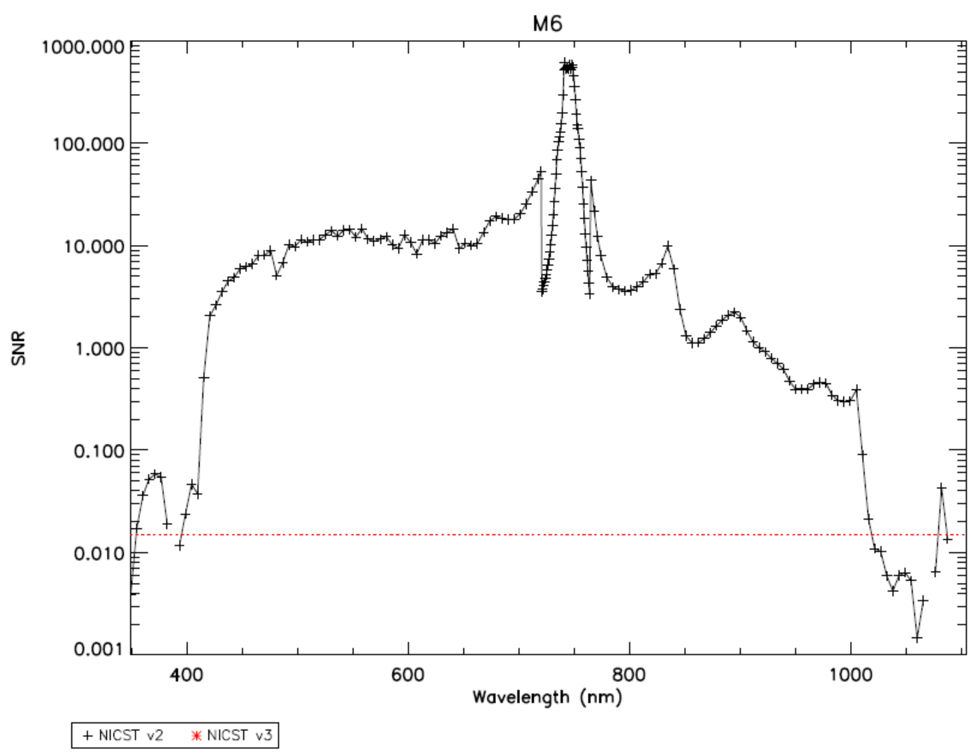

Figure 23: M7 RSR from NICST versions 2 and 3

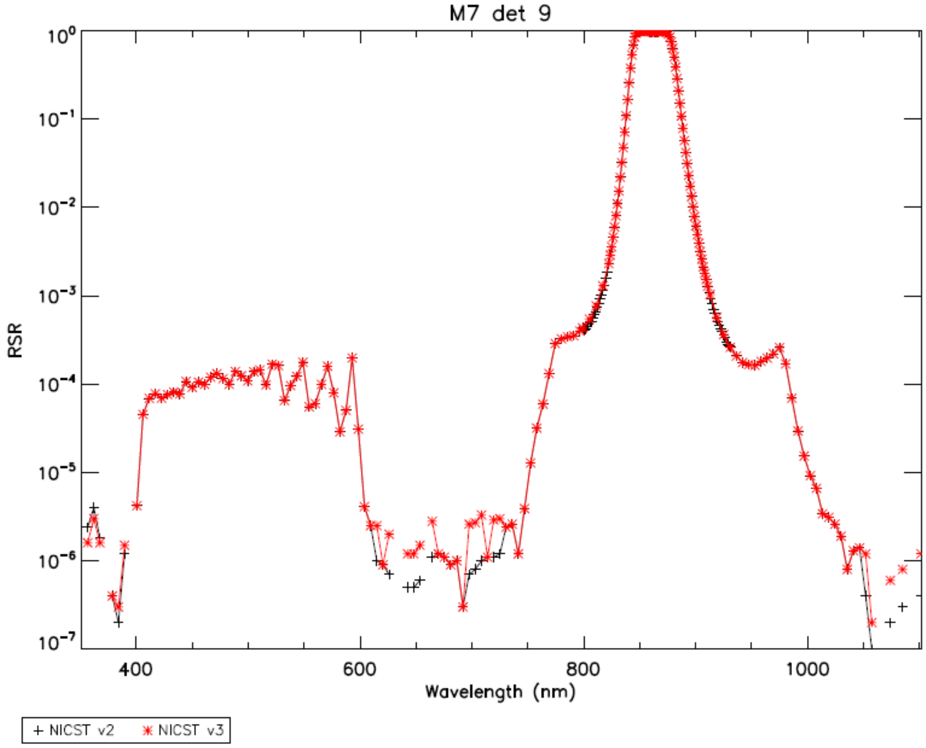

Figure 24: M7 band averaged SNR from NICST version 3

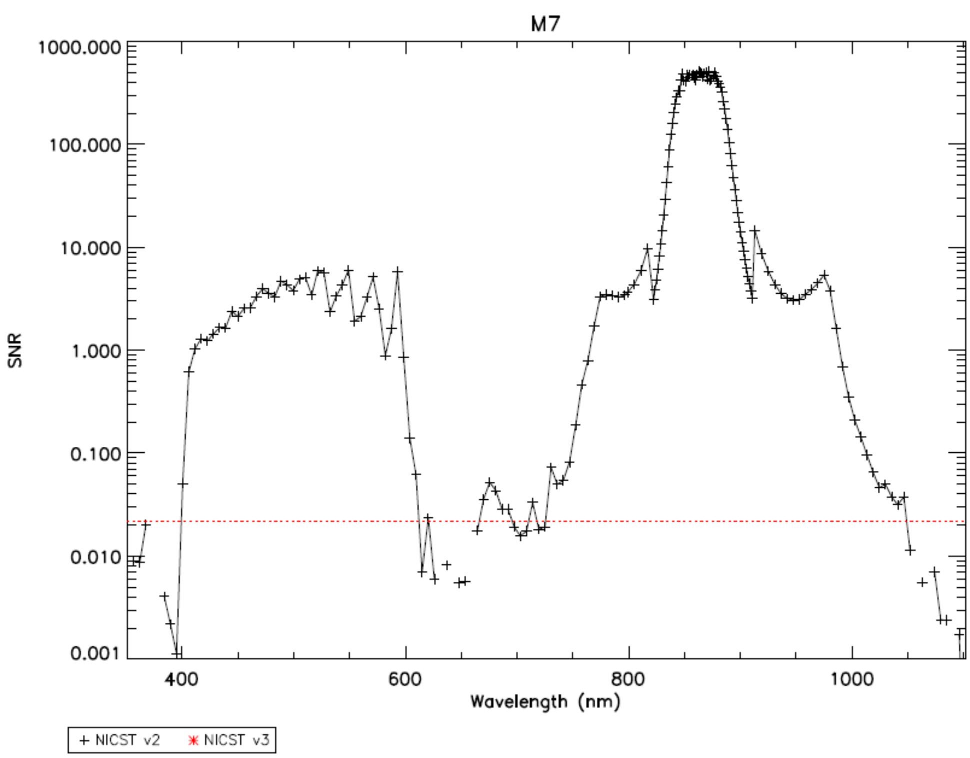

Figure 25: M8 RSR from NICST versions 2 and 3

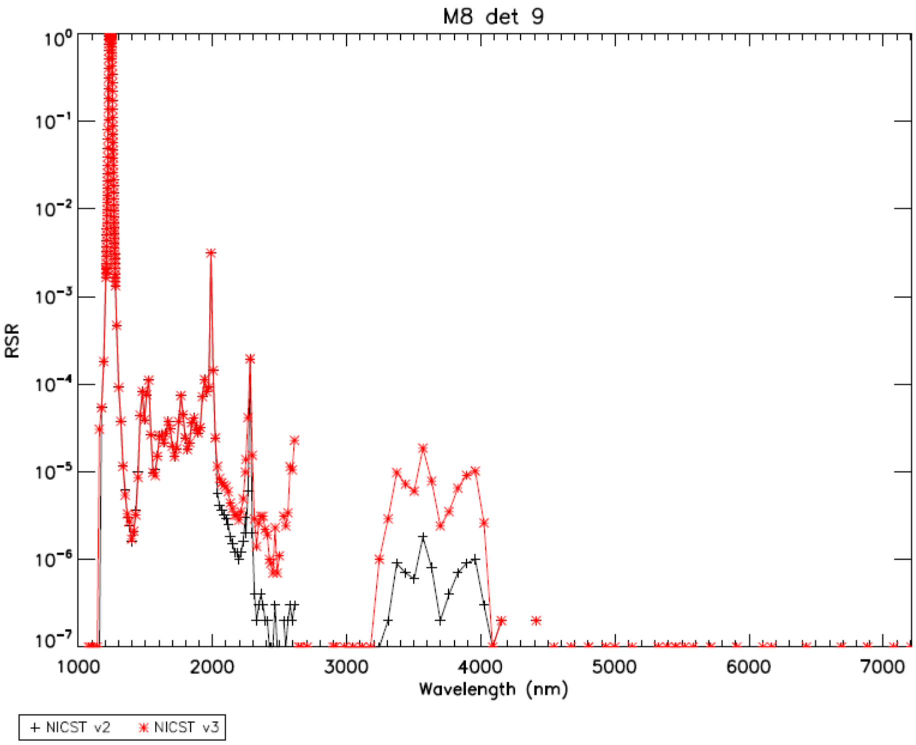

Figure 26: M8 band averaged SNR from NICST version 3

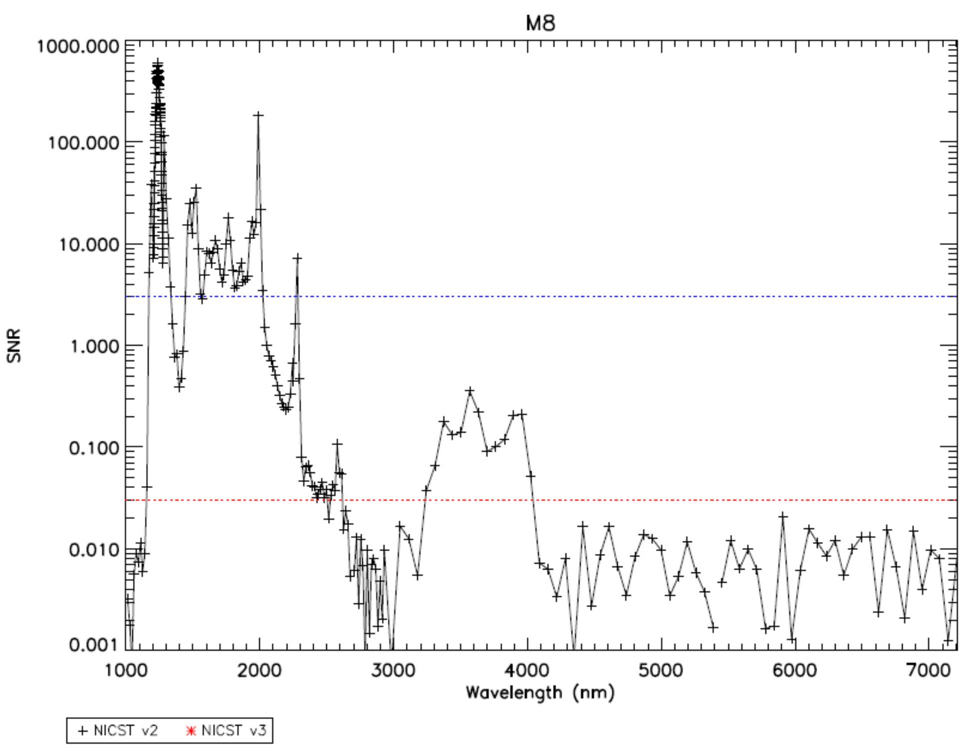

Figure 27: M9 RSR from NICST versions 2 and 3

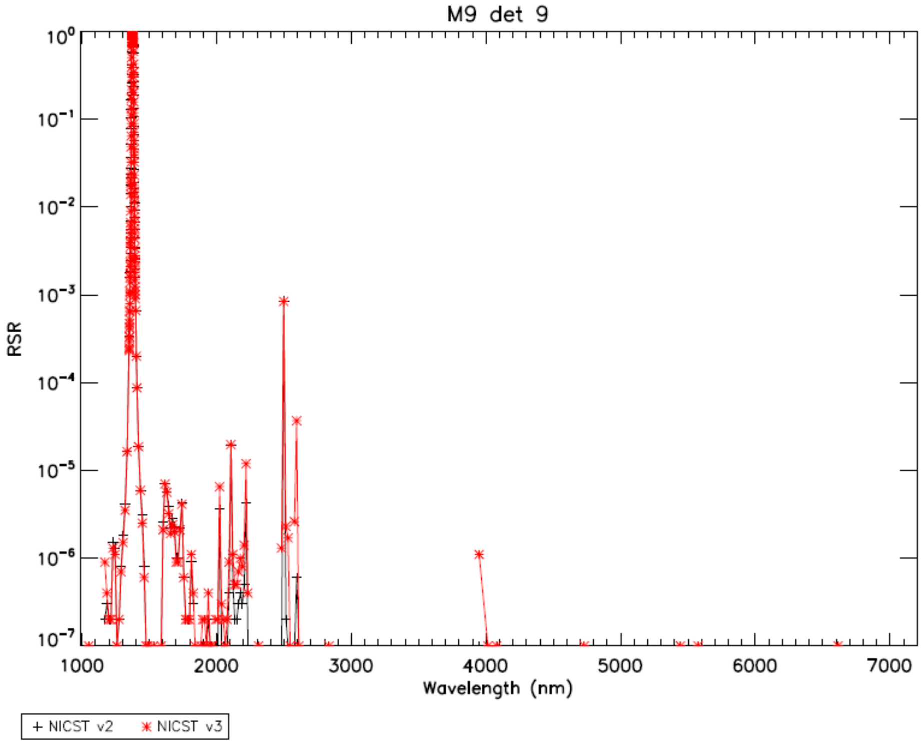

Figure 28: M9 band averaged SNR from NICST version 3

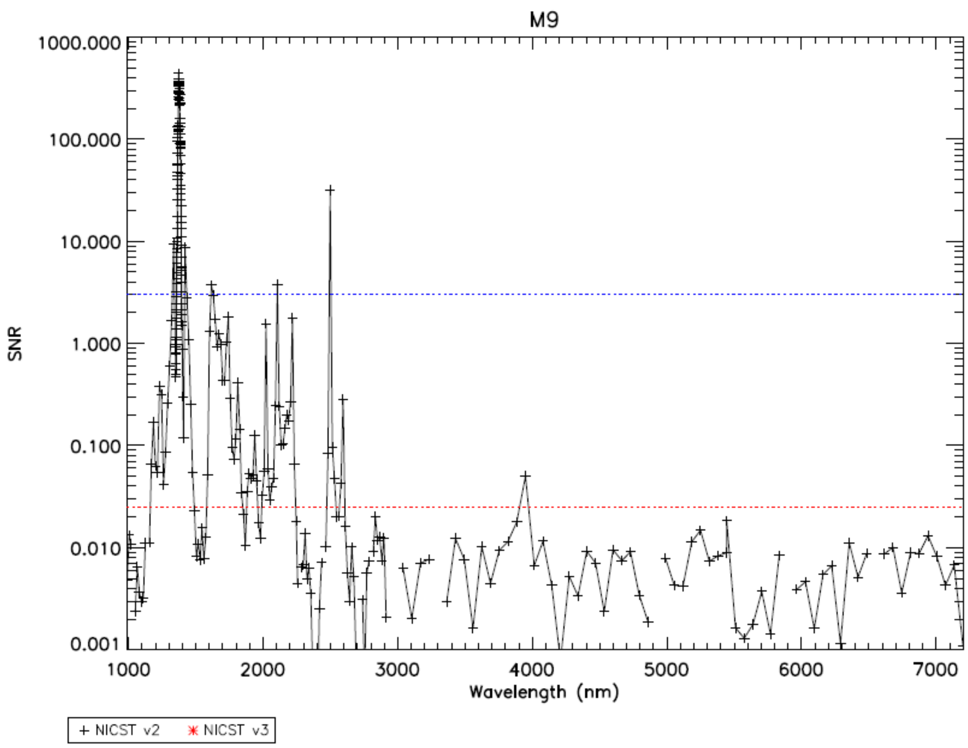

Figure 29: M10 RSR from NICST versions 2 and 3

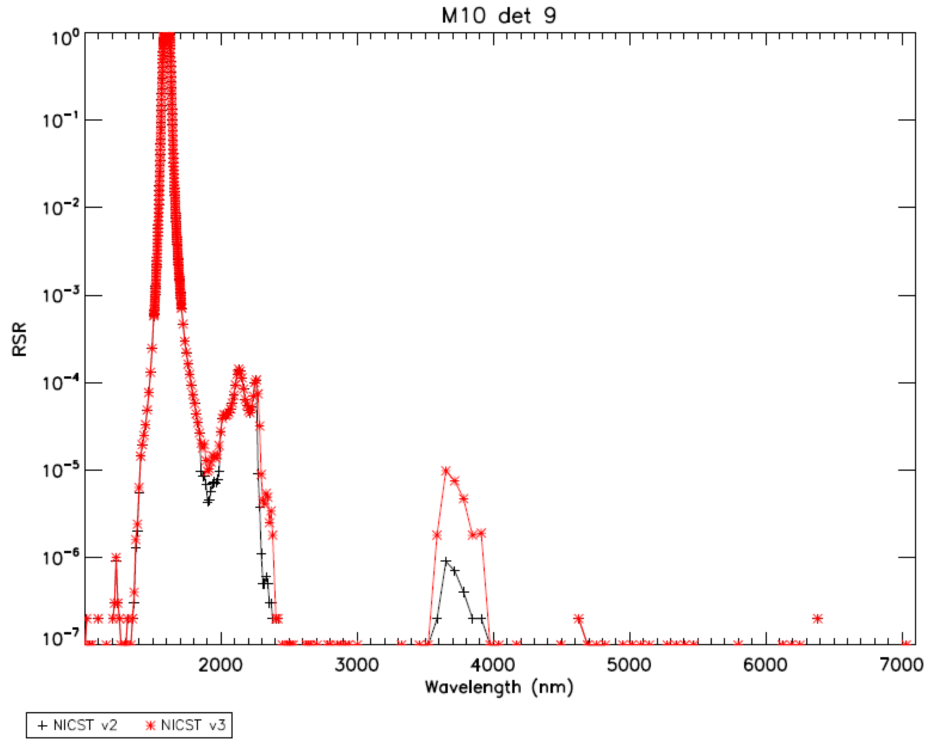

Figure 30: M10 band averaged SNR from NICST version 3

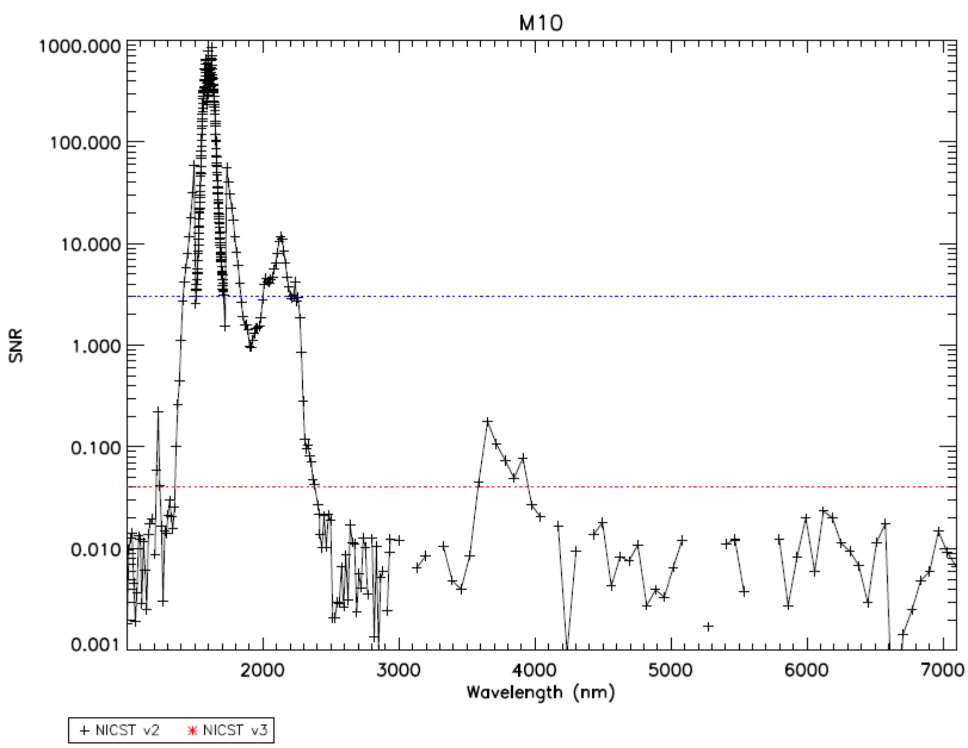

Figure 31: M11 RSR from NICST versions 2 and 3

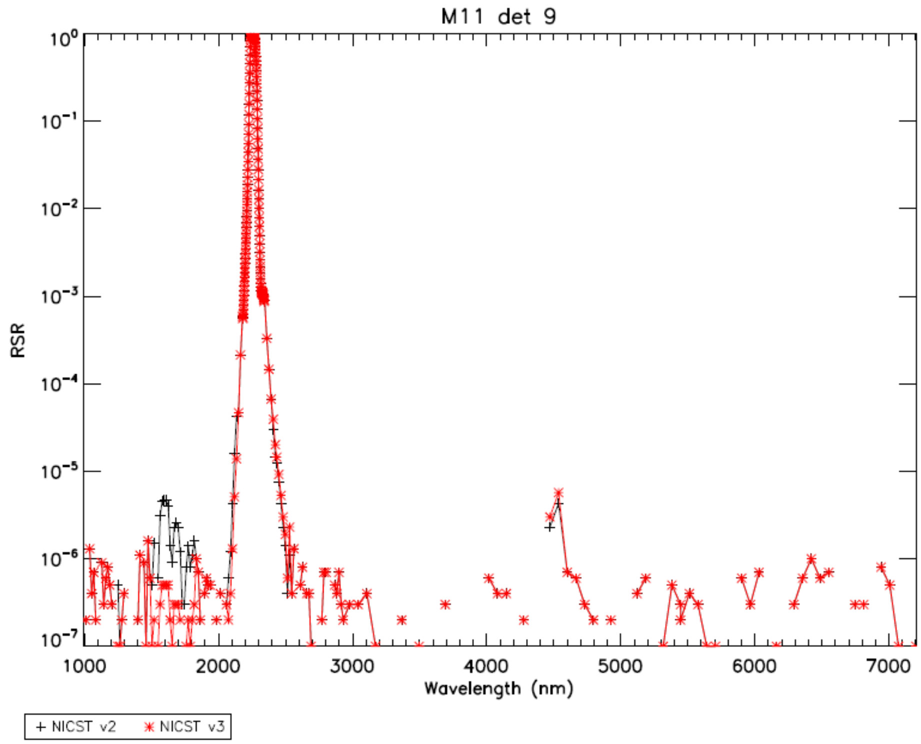

Figure 32: M11 band averaged SNR from NICST version 3

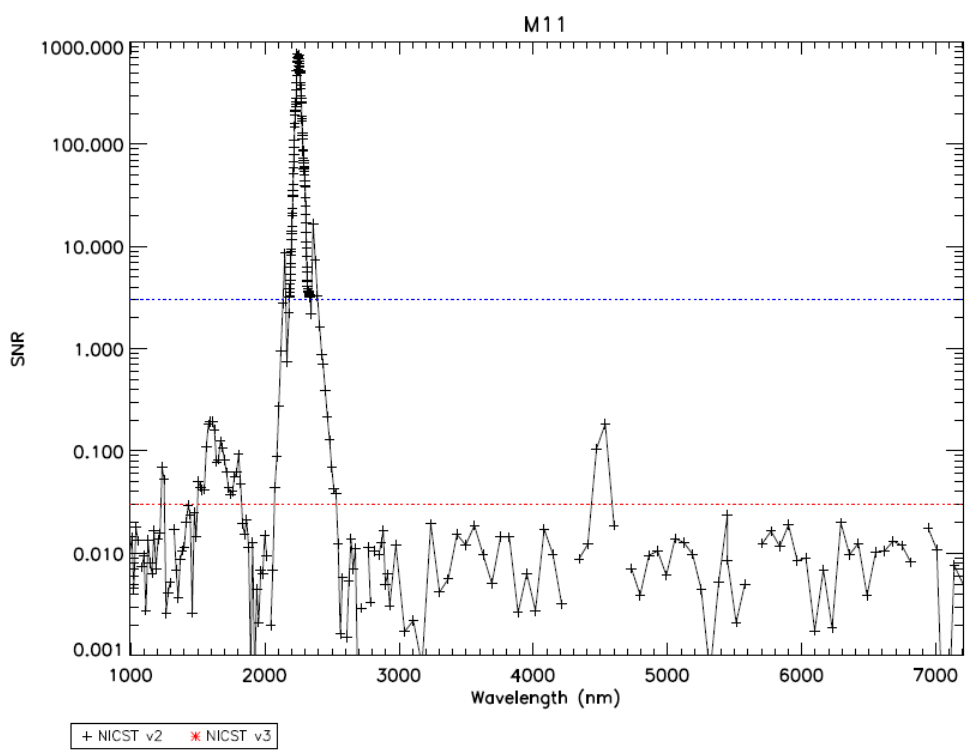

Figure 33: M12 RSR from NICST versions 2 and 3

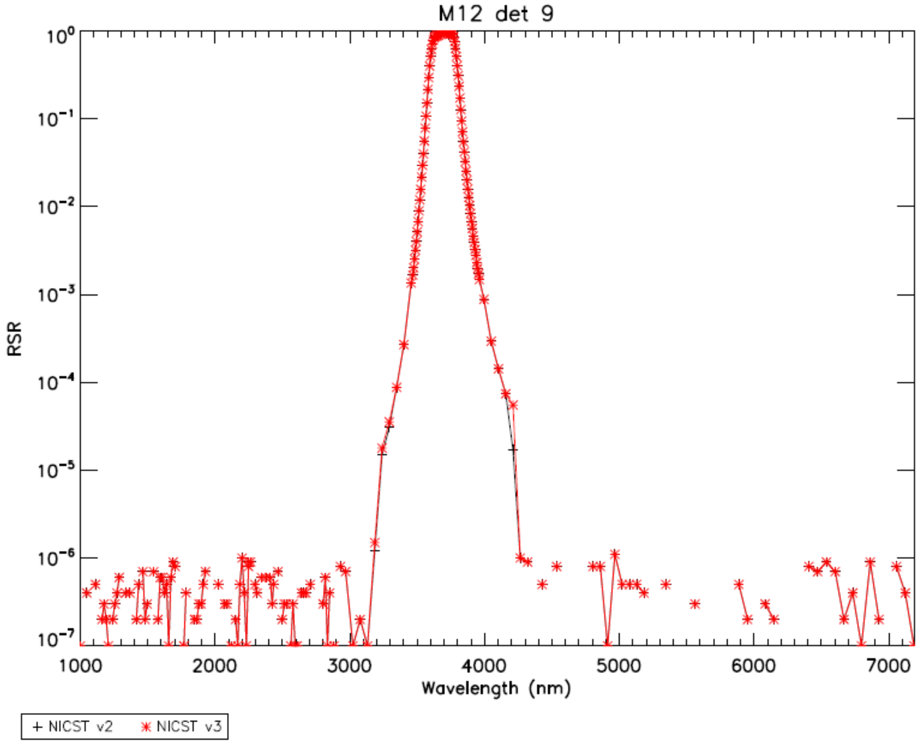

Figure 34: M12 band averaged SNR from NICST version 3

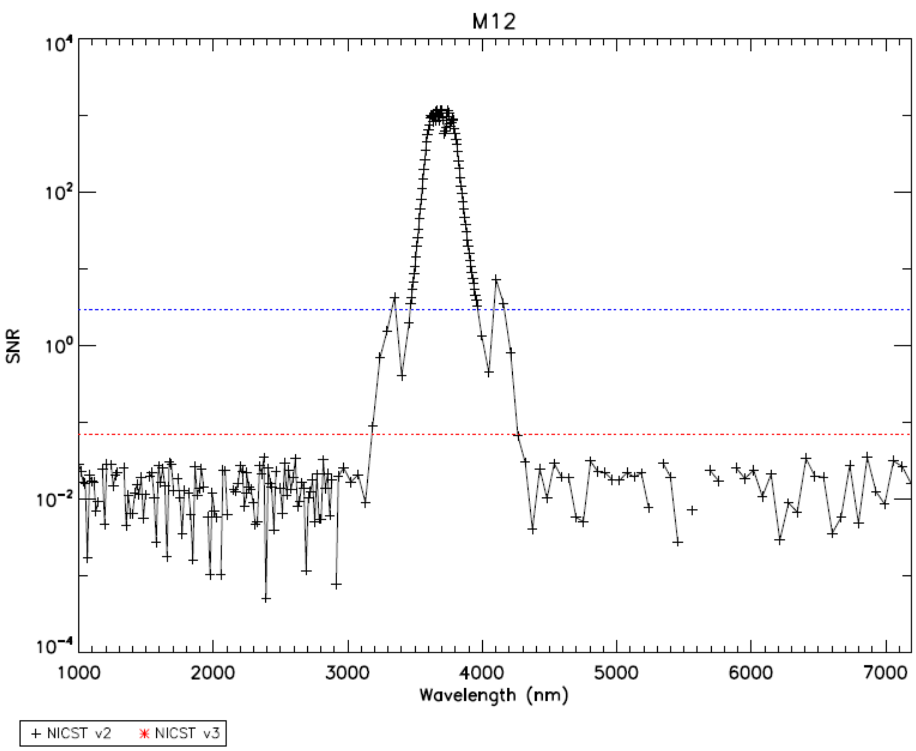

Figure 35: M13 RSR from NICST versions 2 and 3

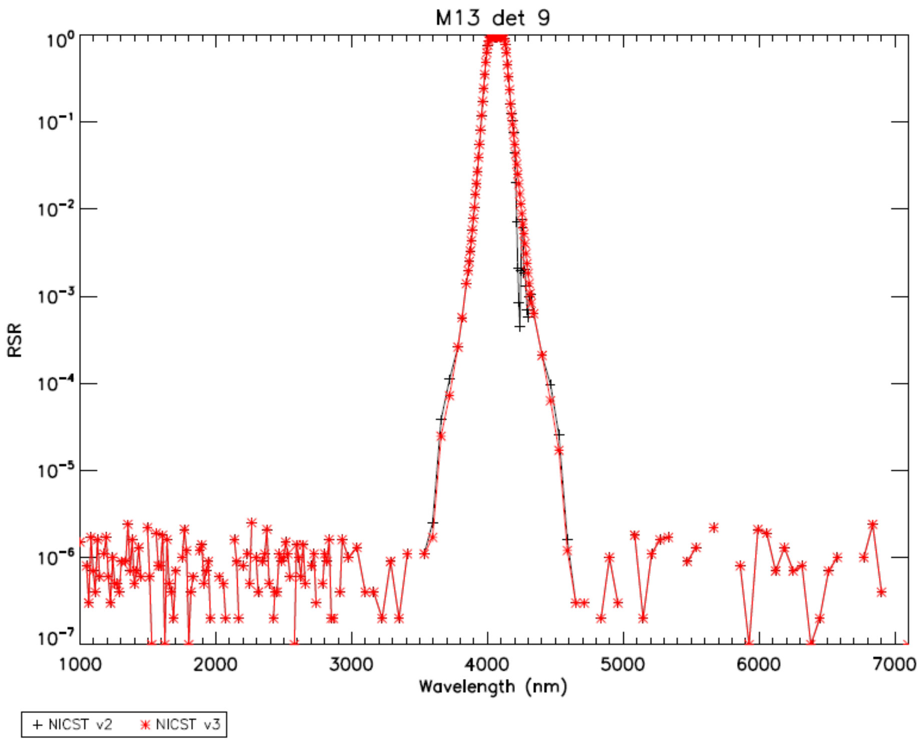

Figure 36: M13 band averaged SNR from NICST version 3

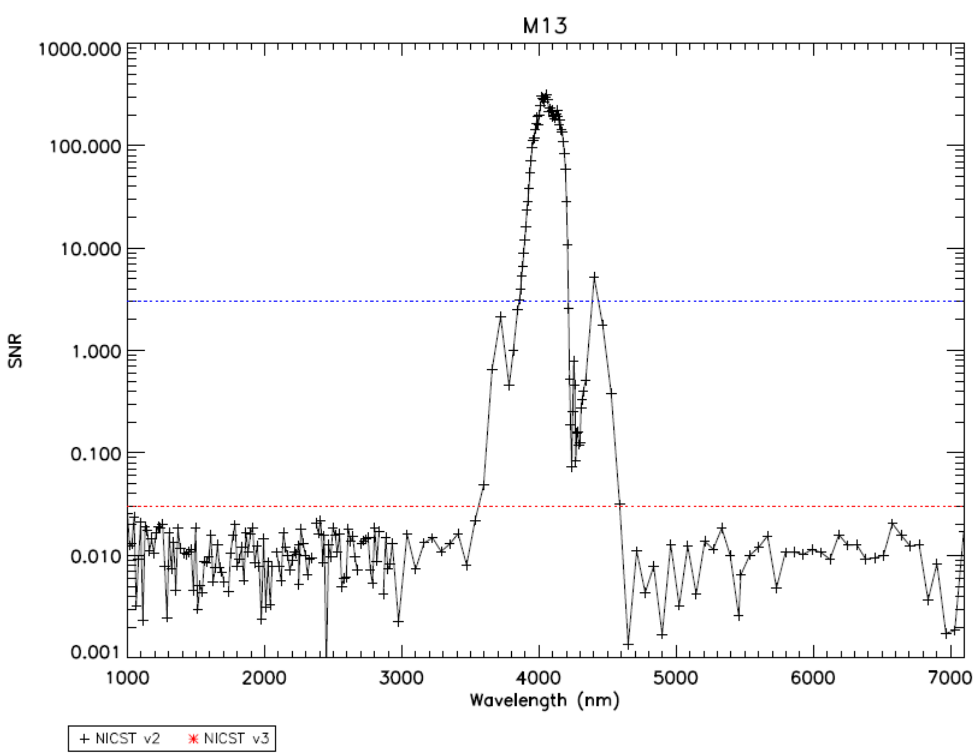

Figure 37: M14 RSR from NICST versions 2 and 3

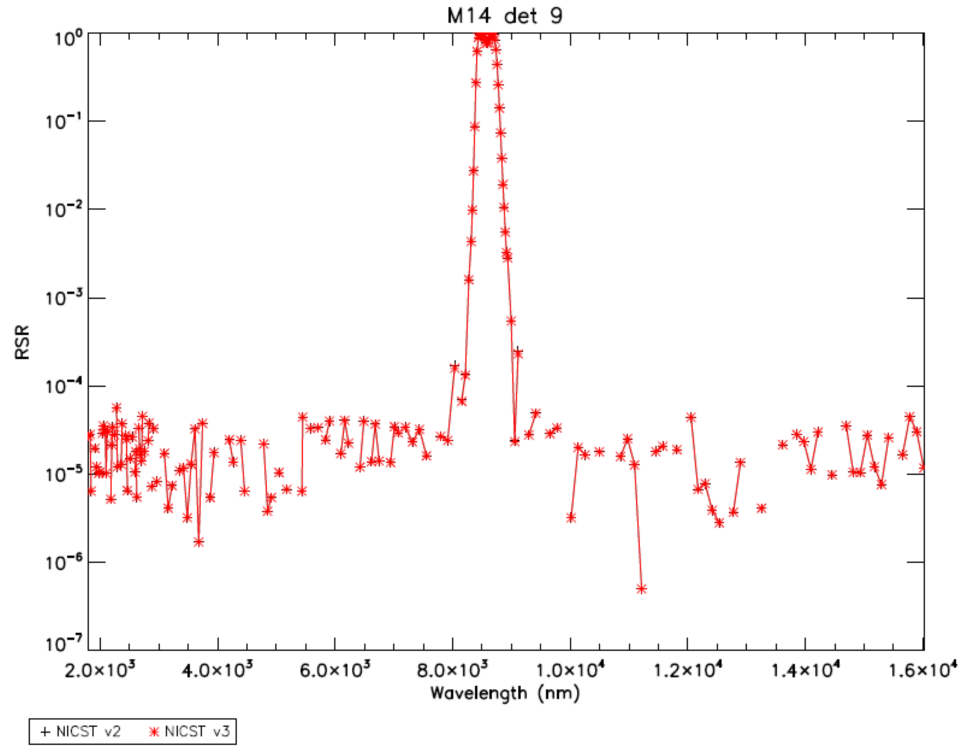

Figure 38: M14 band averaged SNR from NICST version 3

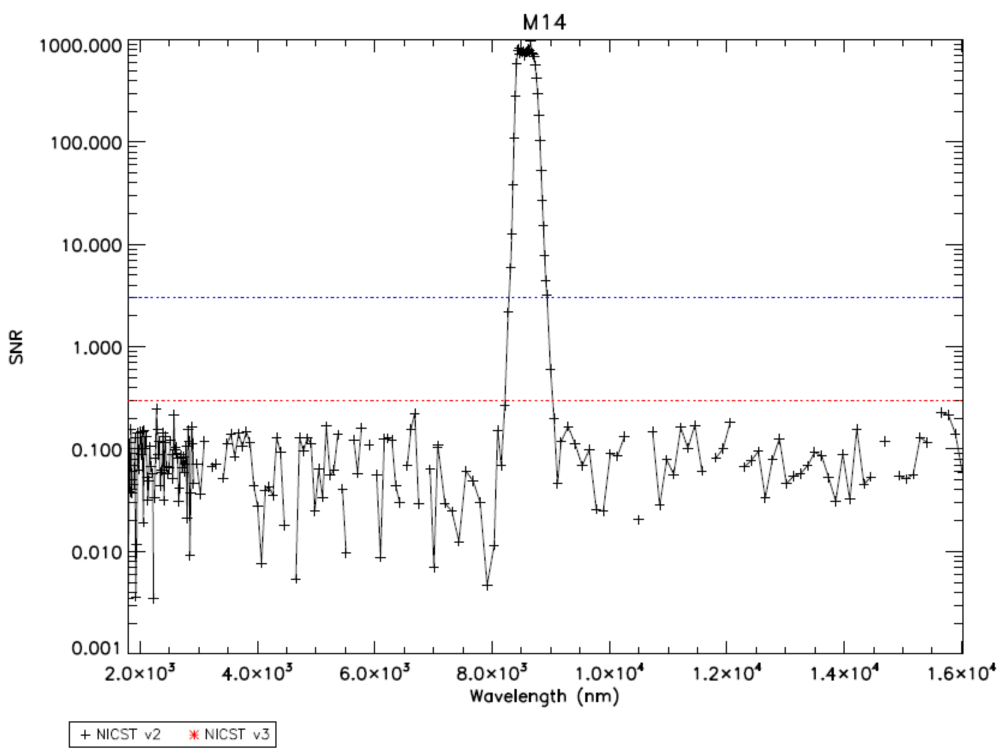

Figure 39: M15 RSR from NICST versions 2 and 3

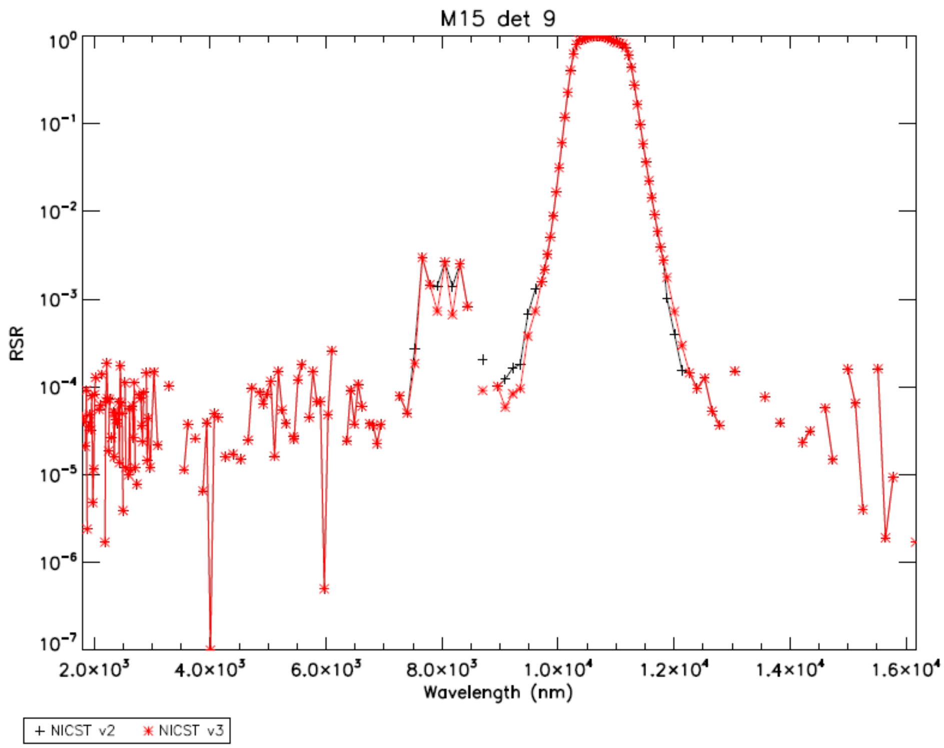

Figure 40: M15 band averaged SNR from NICST version 3

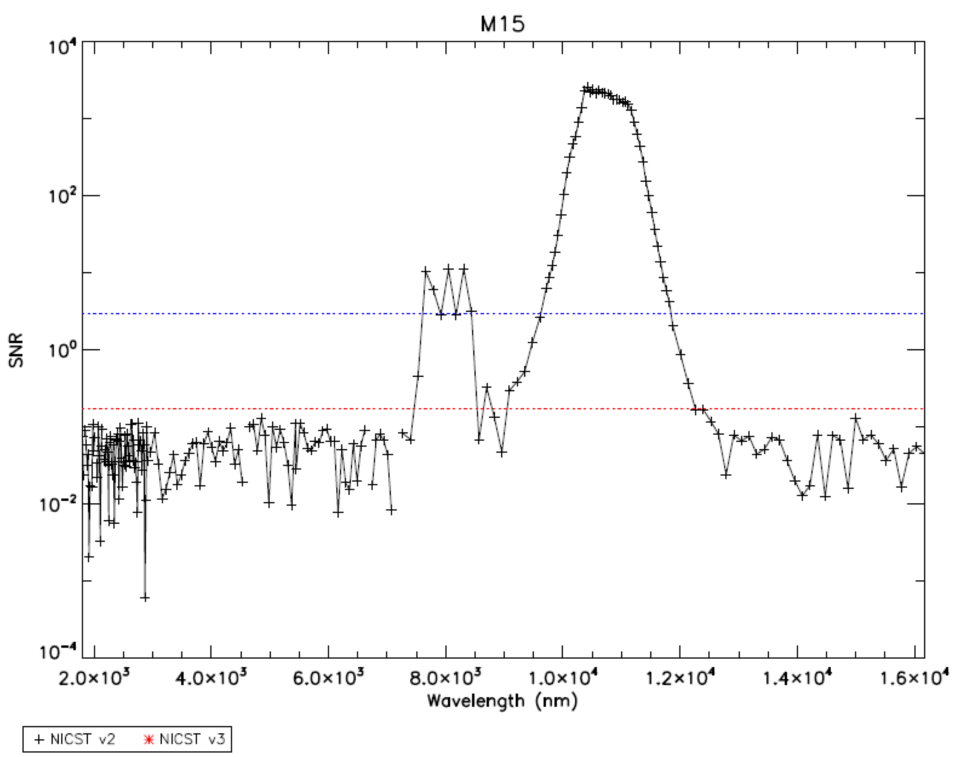

Figure 41: M16A RSR from NICST versions 2 and 3

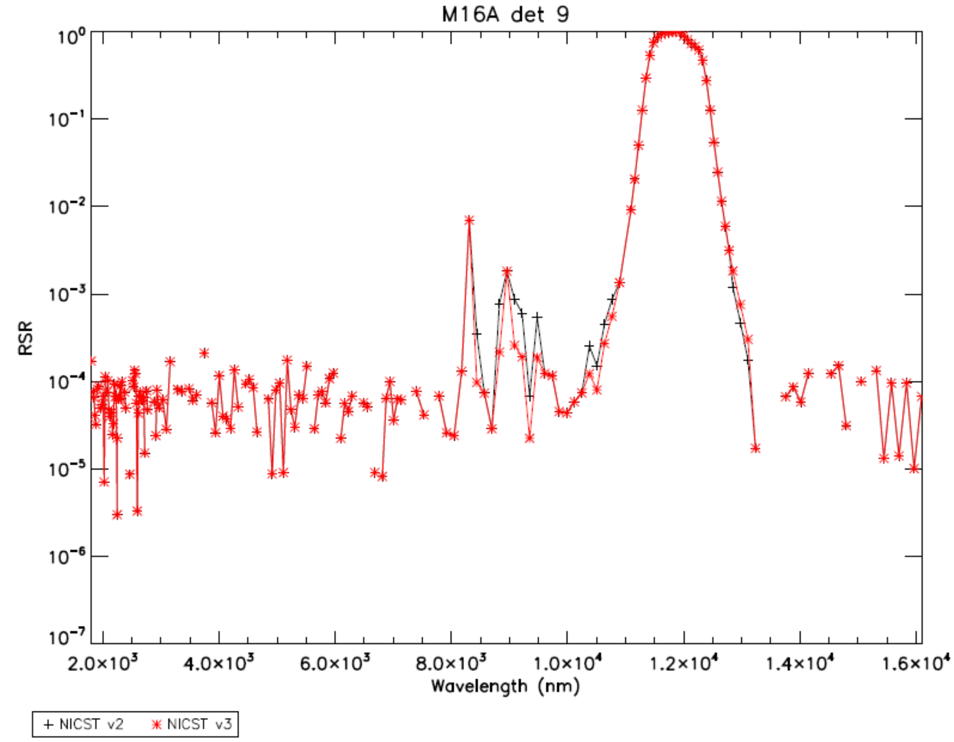

Figure 42: M16A band averaged SNR from NICST version 3

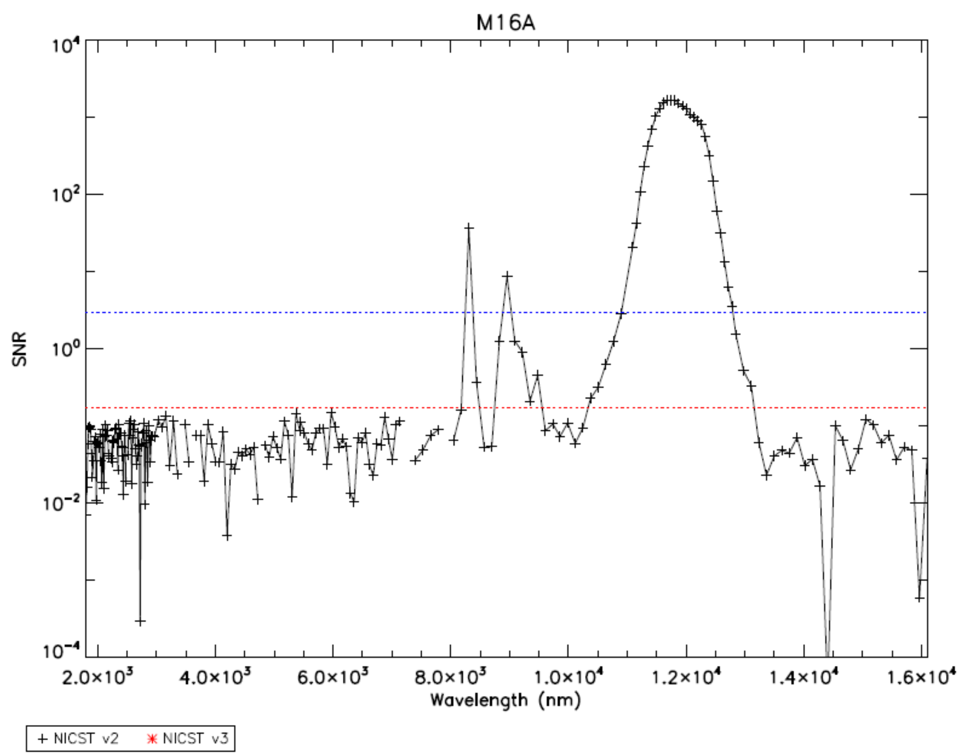

Figure 43: M16B RSR from NICST versions 2 and 3

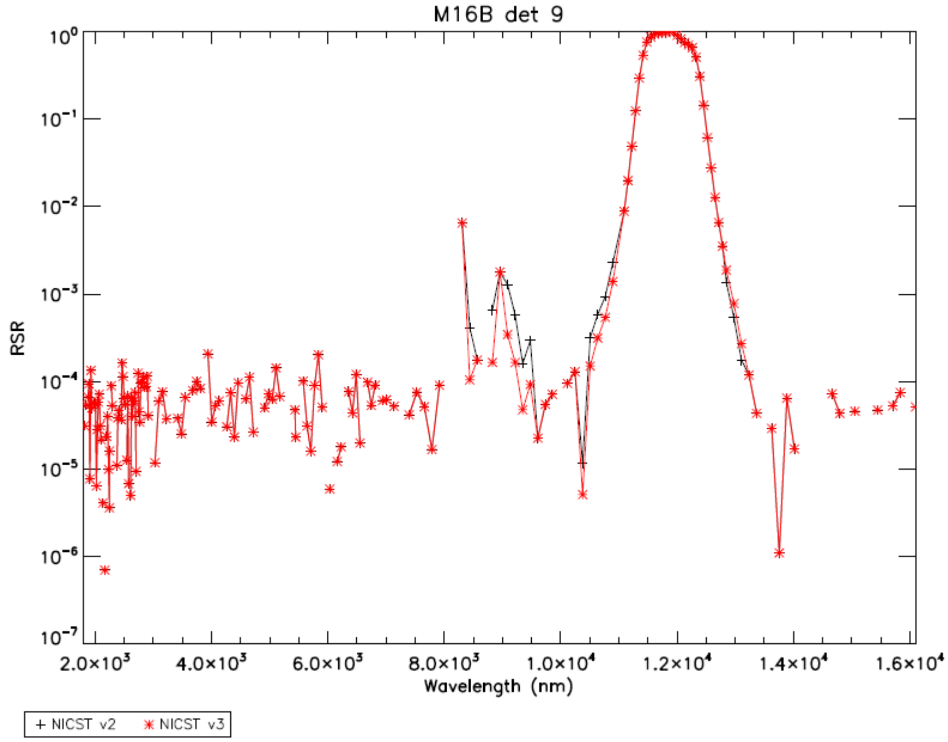

Figure 44: M16B band averaged SNR from NICST version 3

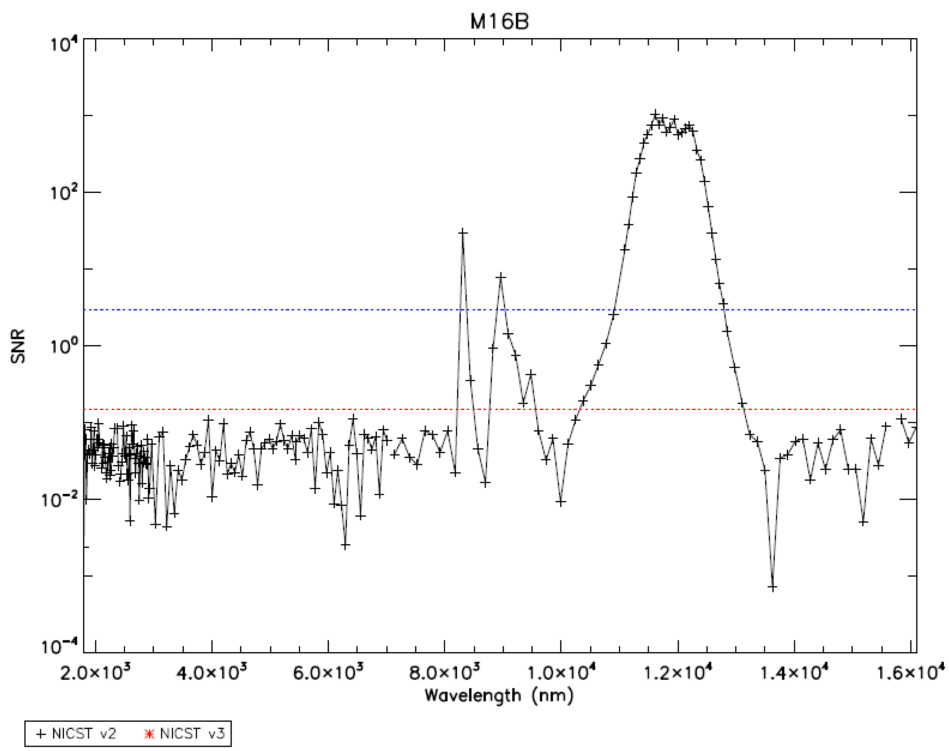

Figure 45: Atmospheric correction for M9 detector 9

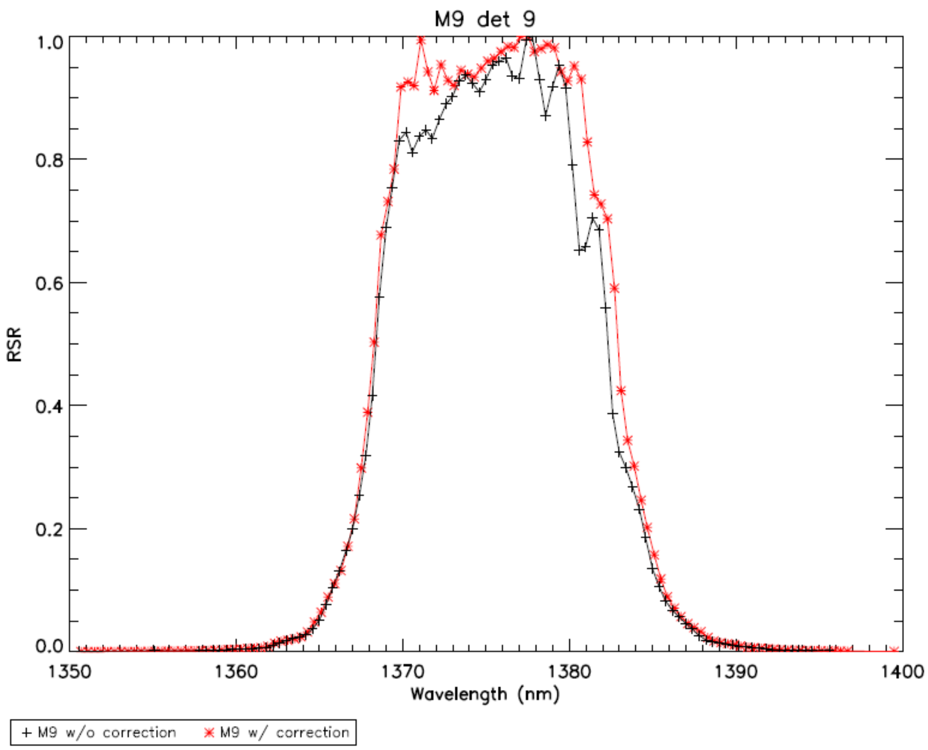

Figure 46: Stitching improvement for M9 detector 9

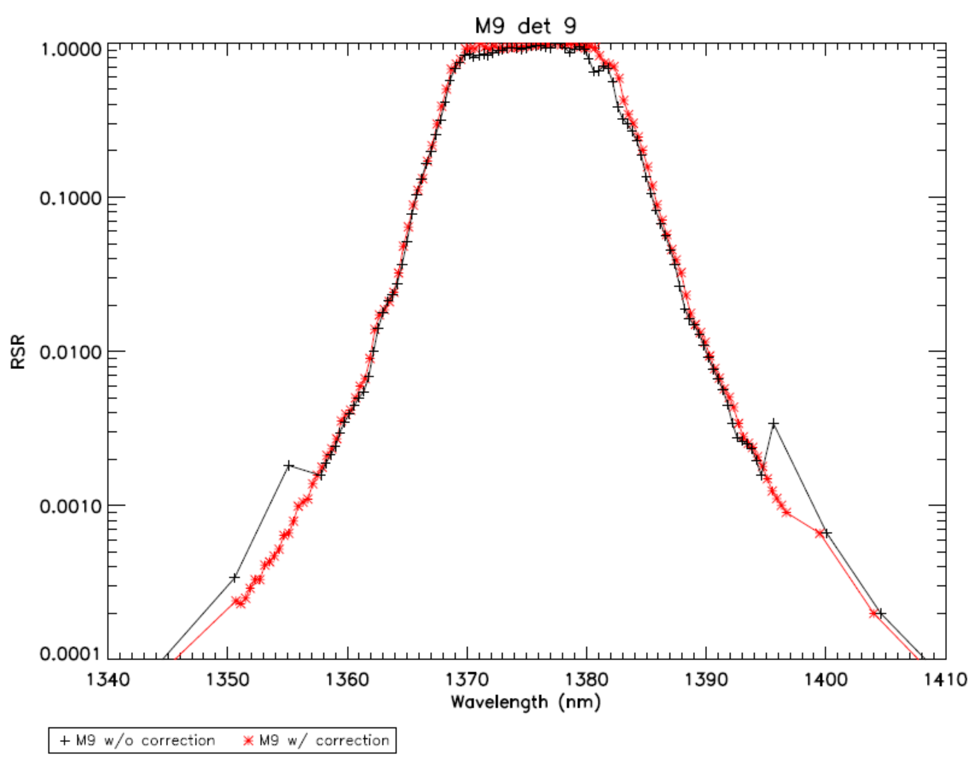

Figure 47: M13 atmospheric feature with absorption spectrum

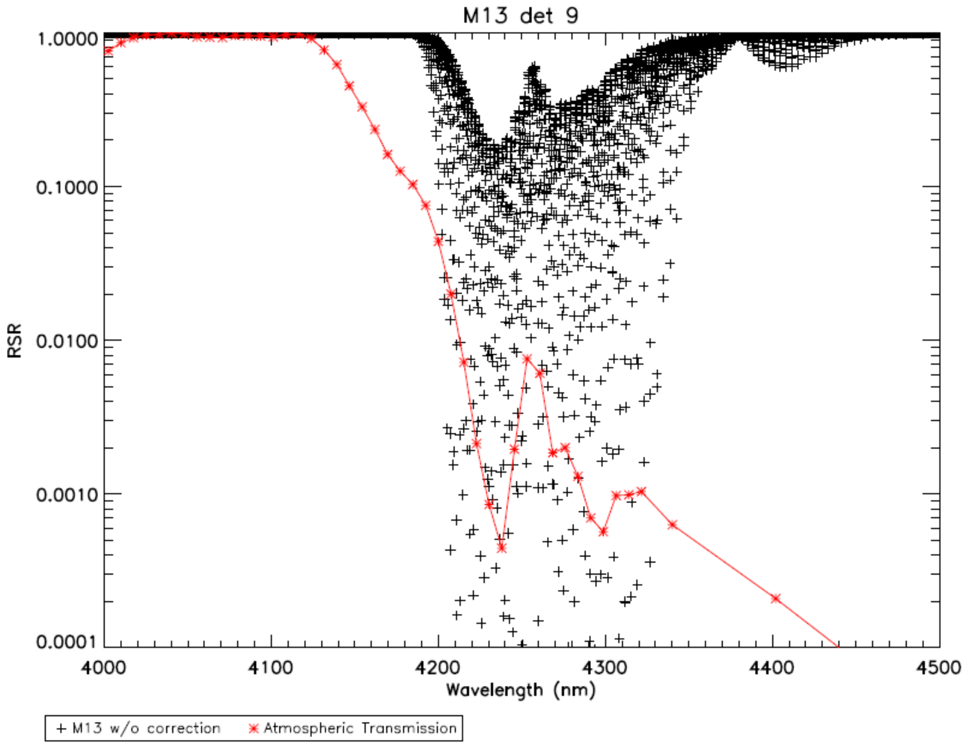

Figure 48: M13 atmospheric correction

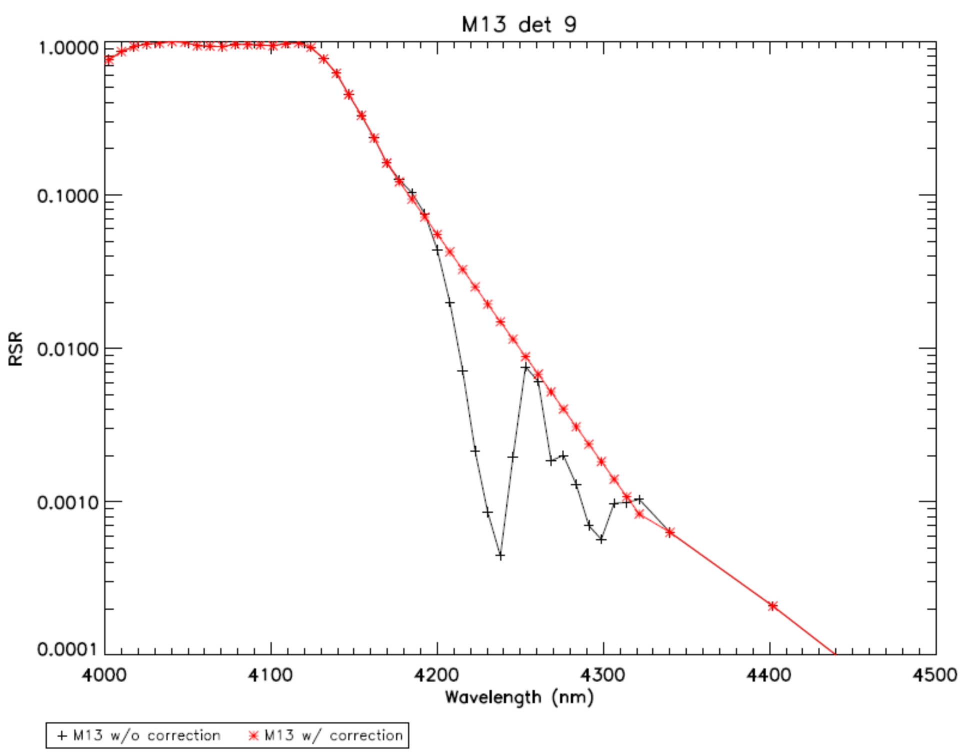

Figure 49: Stitching of FP-15 to FP-16 for I1

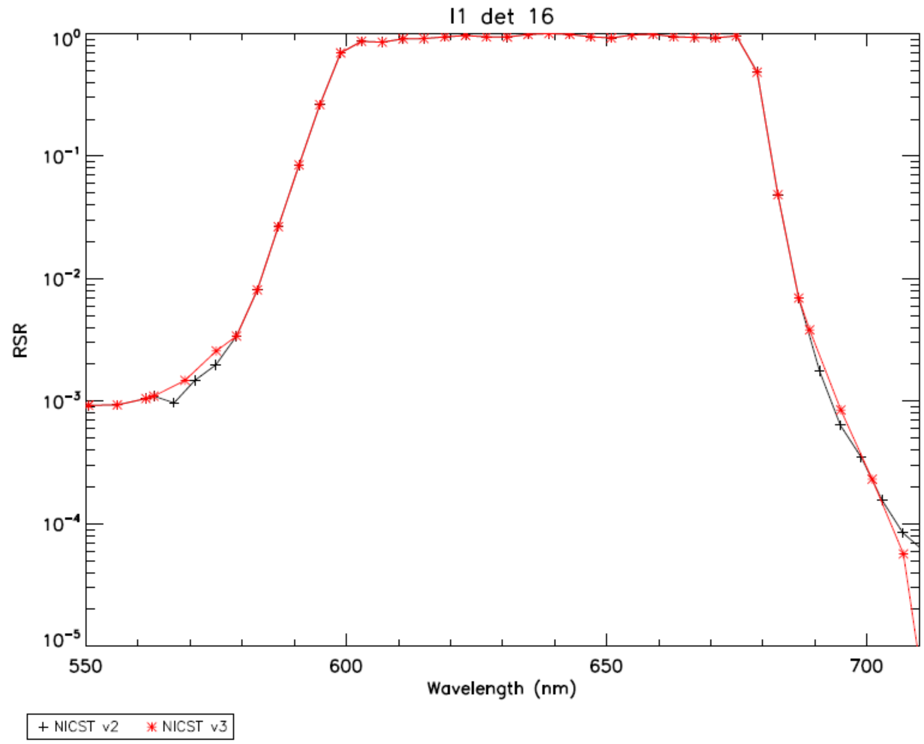

Figure 50: Stitching of FP-15 to FP-16 for M2

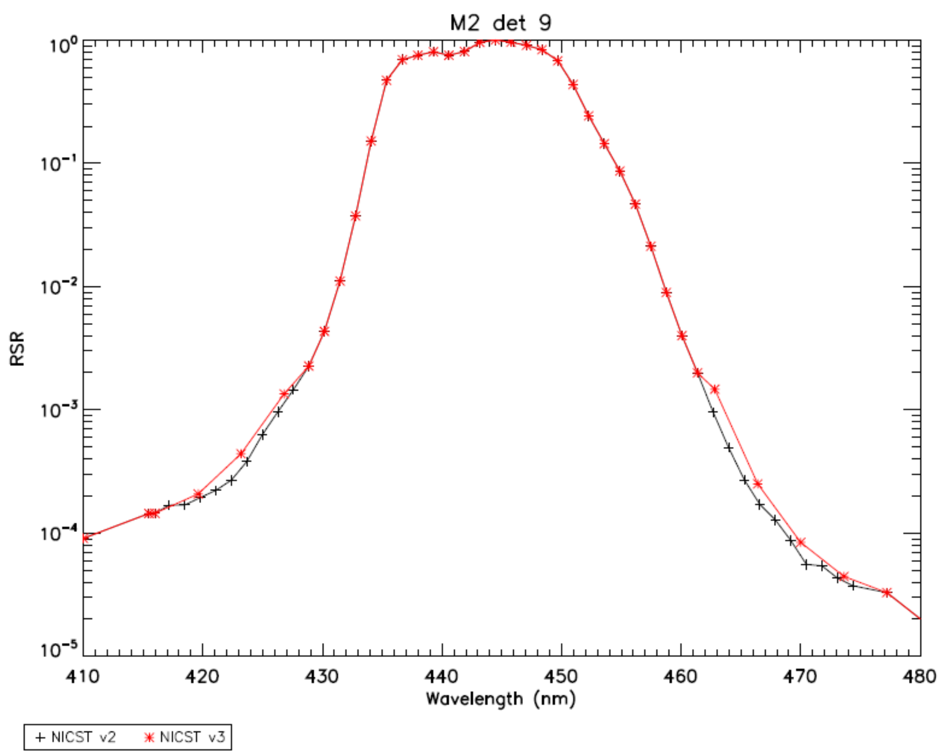

Figure 51: Stitching of FP-15 to FP-16 for M3

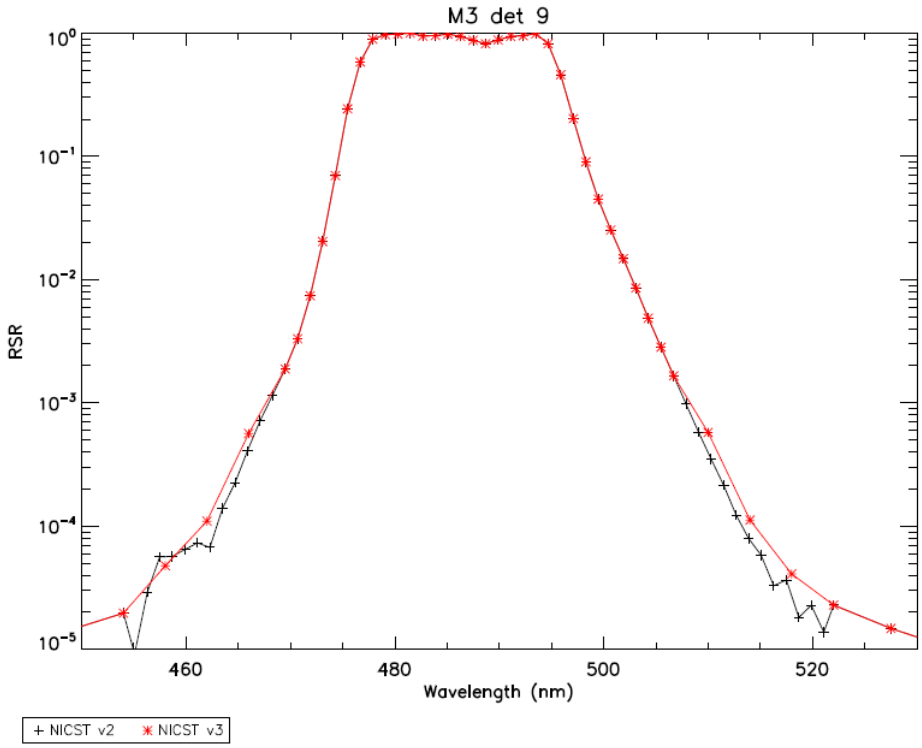

Figure 52: Stitching of FP-15 to FP-16 for M7

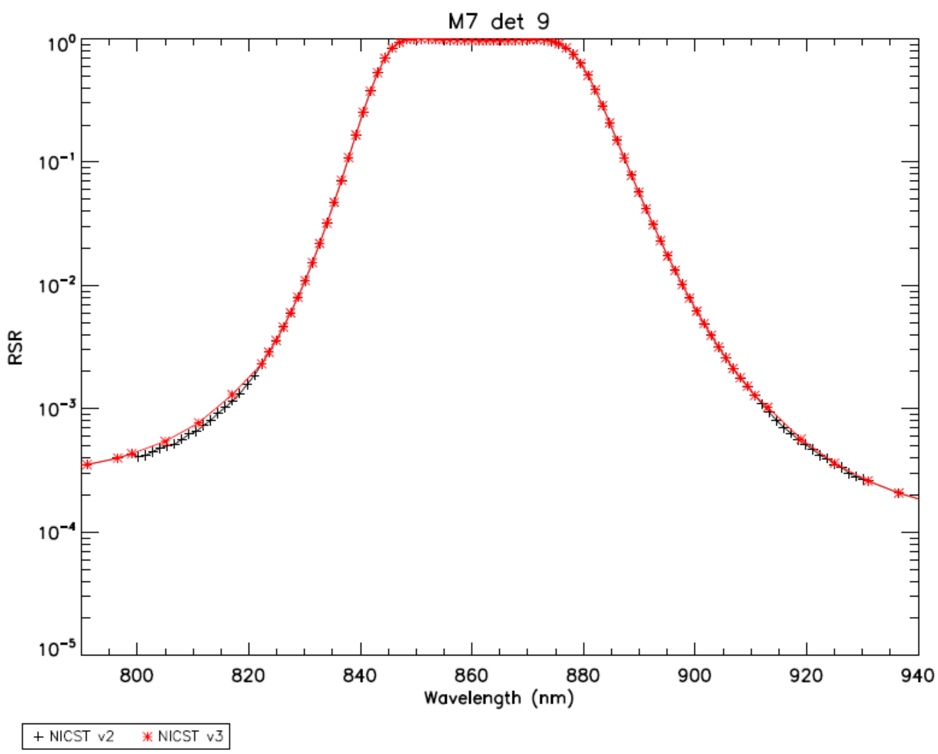

Figure 53: M12 detector 1 RSR

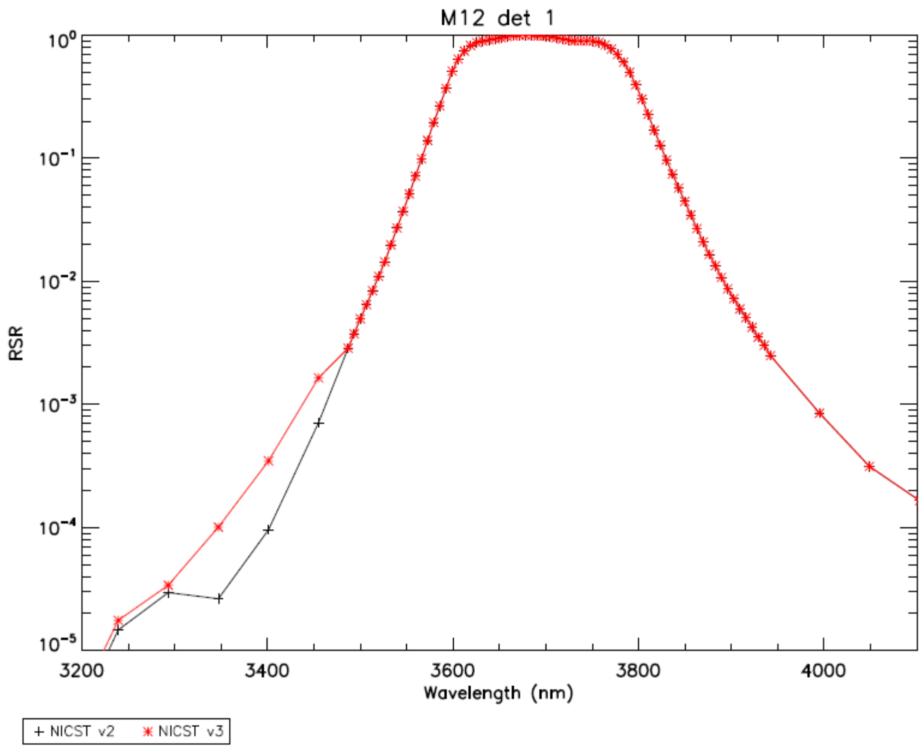

Figure 54: IOOB from NICST RSR versions 2 and 3

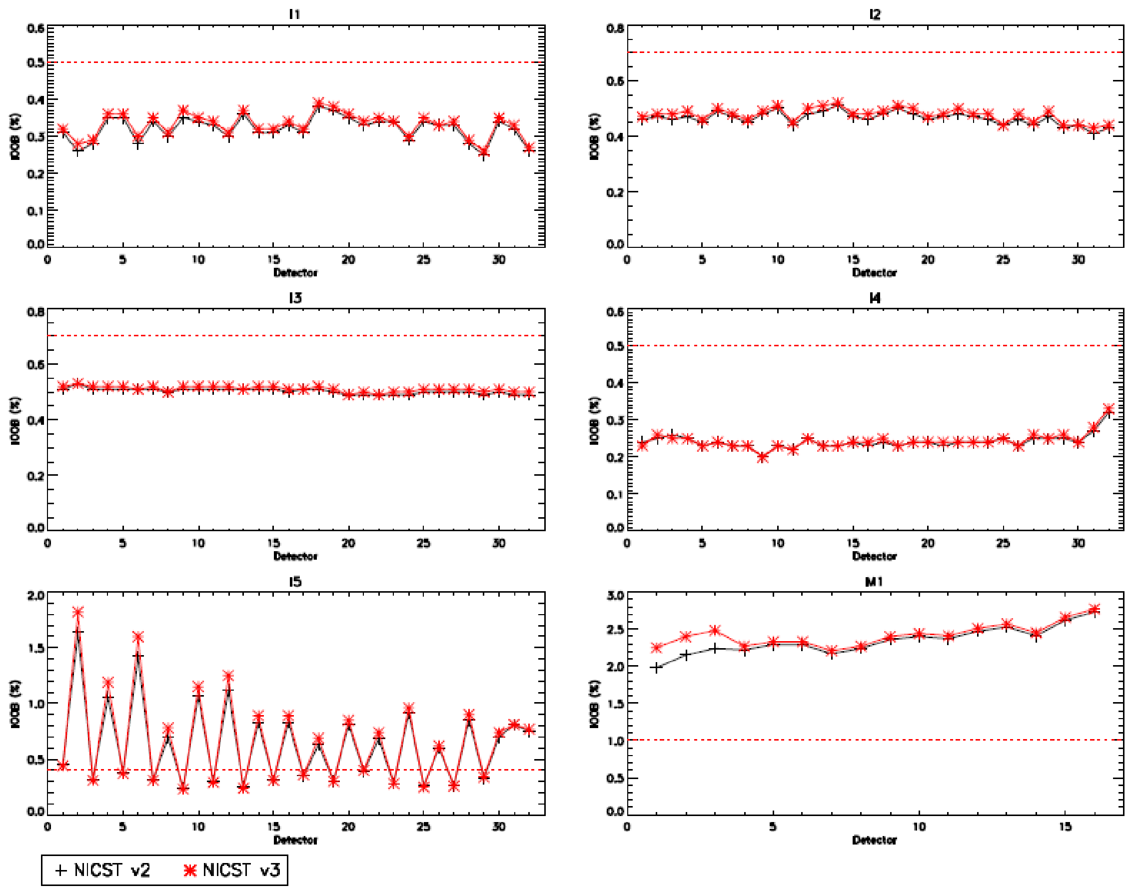

Figure 55: IOOB from NICST RSR versions 2 and 3

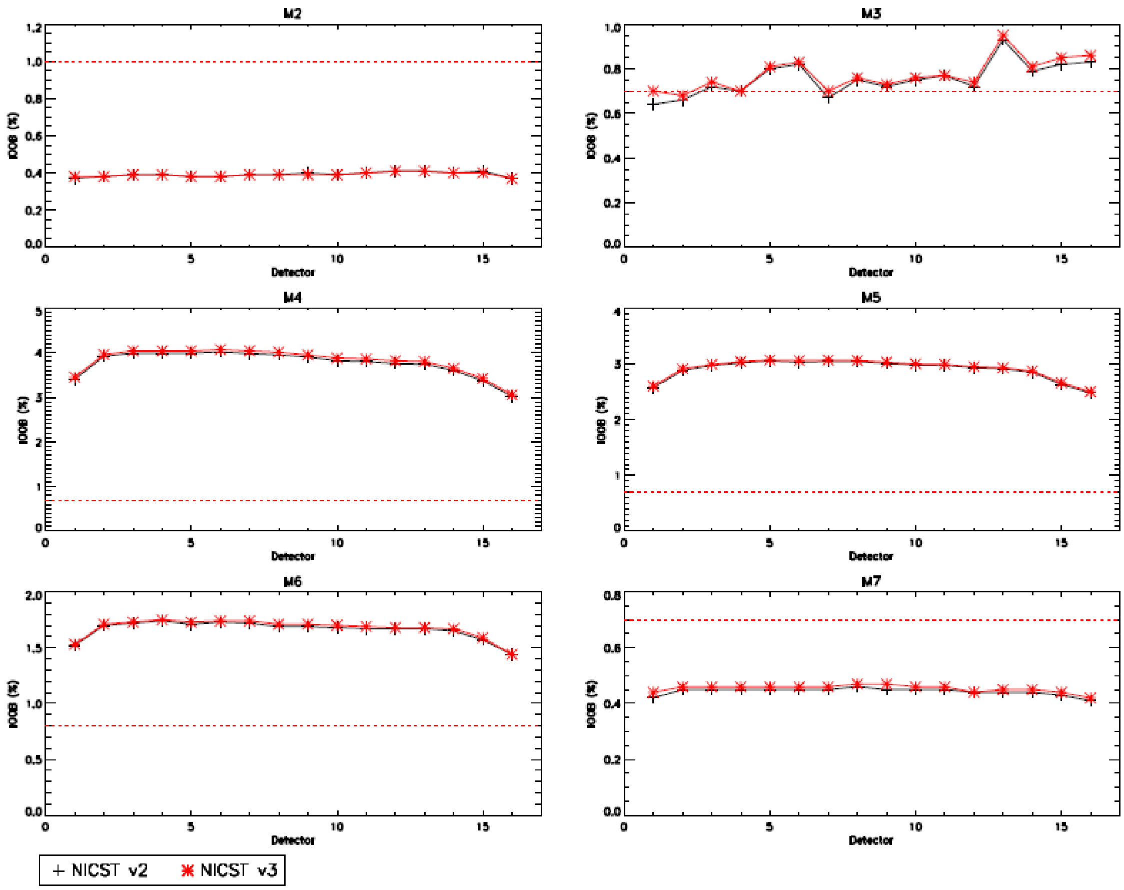

Figure 56: IOOB from NICST RSR versions 2 and 3

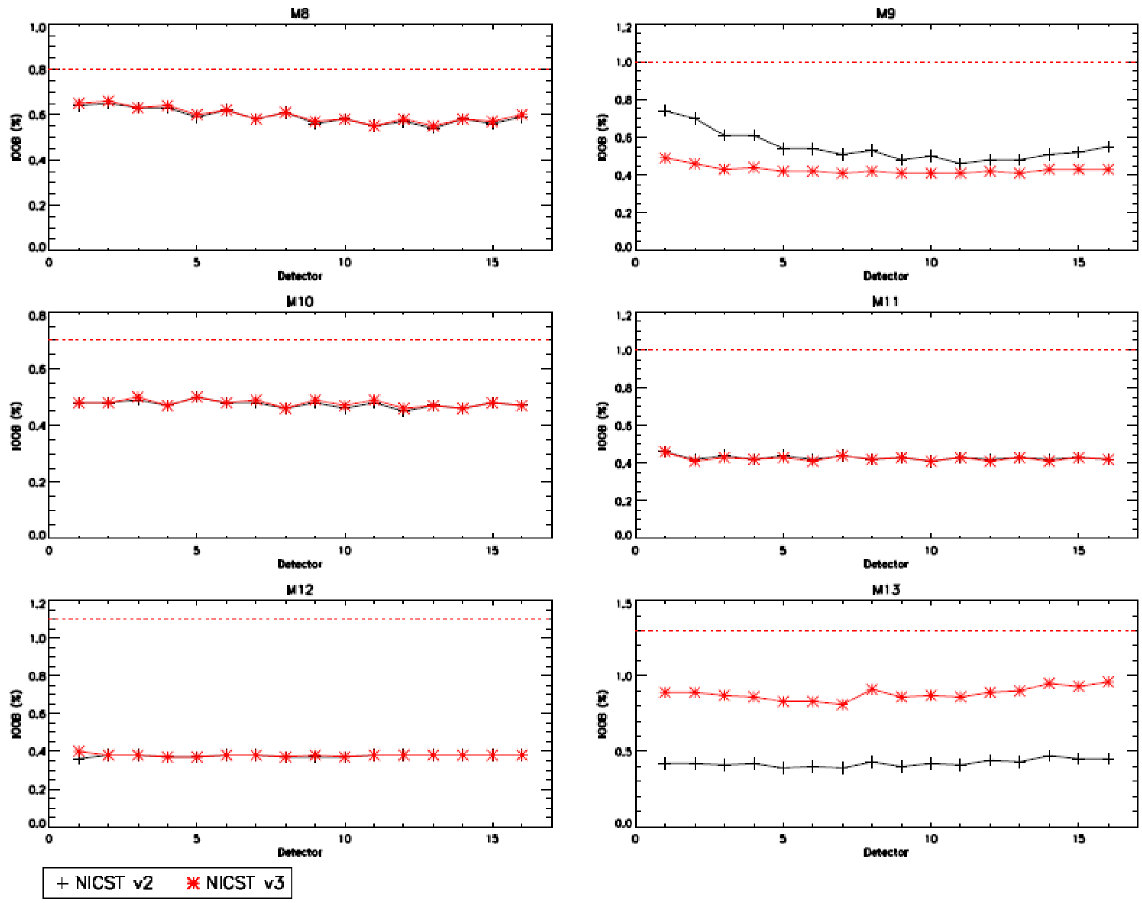

Figure 57: IOOB from NICST RSR versions 2 and 3